Université du Québec
à Rimouski

Étude de la chimie des carbonates le long d'un petit continuum rivière - océan côtier

Mémoire présenté

dans le cadre du programme de maîtrise en océanographie

en vue de l'obtention du grade de maître ès sciences

PAR

© Olivier Turcotte

Avril 2025

Composition du jury :

André Pellerin, présidence du jury, UQÀR-ISMER

Gwénaëlle Chaillou, direction de recherche, UQÀR-ISMER

Fanny Noisette, codirection de recherche, UQÀR-ISMER

Alfonso Mucci, codirection de recherche, Université McGill

Richard St-Louis, examinateur externe, UQÀR

Dépôt initial le 5 décembre 2024 Dépôt final le 11 avril 2025

Votre dur labeur sera bientôt récompensé.

- Biscuit de fortunes

REMERCIEMENTS

Ce mémoire est le produit d'une construction collective, et cette mosaïque de support se doit d'être soulignée. Tout d'abord, je désire remercier Gwénaëlle pour l'accueil au sein de son équipe de recherche et les opportunités qu'elle m'a offertes tout au long de ma maîtrise. Merci également pour ta patience et ton support, malgré plusieurs détours. On aura réussi à maintenir le cap afin de compléter ce projet.

Merci, Fanny, pour ta disponibilité afin de réfléchir à haute voix sur bien des affaires, ces échanges ont été essentiels. Merci, Alfonso, pour tes conseils et connaissances sur les carbonates. Cette expertise a été essentielle. Merci à ce trio pour leurs corrections et commentaires tout au long de ce travail.

Je veux remercier les collègues et ami·es qui ont fait partie de cette aventure, à Rimouski au labo; Éléonore, Carole-Anne, Aude, Gwendoline, Félix, Antoine, Ludovic, Alice et Laísa qui m'ont apporté leur support et connaissances tant au niveau des campagnes de terrain, du laboratoire et du monde de la recherche. Merci à Steeven pour son support au laboratoire de chimie, à Bruno, Fred et Christian pour leur support technique et sur le terrain. Merci aux collègues d'Halifax pour leur accueil, amitié et support; Doug, Claire, Will, Caroline, Adriana et Marie.

Merci profondément aux ami.es de Rimouski et d'ailleurs, ainsi que la famille pour le support, l'amour et les rires au travers de cette aventure. Ce support a été essentiel afin de compléter ce projet.

RÉSUMÉ

Les échanges gazeux à l'interface air-eau sont dictés par la loi de Henry et la capacité de l'océan global comme puits de CO_2 est maintenant bien documentée. Au contraire, les caractéristiques de puits ou de source nette de CO_2 de l'océan côtier sont encore peu contraintes et sujettes à débats. L'océan côtier est un environnement dynamique quant à la production/consommation de carbone inorganique dissout (DIC pour *dissolved inorganic carbon*) et d'alcalinité totale (TA pour *total alkalinity*) qui influence à son tour la capacité tampon de pH ainsi que les échanges de CO_2. L'objectif général de cette recherche consiste à suivre la distribution saisonnière des paramètres du système des carbonates le long d'un continuum rivière – océan côtier. Plus spécifiquement, le projet consiste à 1) déterminer si les apports latéraux issus d'une rivière et de son estuaire agissent comme puits ou source de CO_2 à l'atmosphère, 2) déterminer si la décharge de la rivière augmente ou diminue la capacité tampon de pH des eaux côtières, et 3) construire un budget de carbone saisonnier le long du continuum rivière – océan côtier. La rivière Kamouraska, dans l'ouest du Bas-Saint-Laurent (Québec, Canada), a été sélectionnée comme un modèle d'un petit affluent de l'estuaire supérieur du Saint-Laurent. Les eaux de surface ont été prélevées le long du gradient de salinité, de la rivière à l'estuaire supérieur, et les paramètres du système des carbonates (pH, TA, DIC, pression partielle de CO_2) ont été mesurés en mai, juillet, août et octobre 2022, lors de la saison libre de glace. Les flux de CO_2 vers l'atmosphère varient entre 94 ± 68 et 958 ± 238 $\mu mol\ m^{-2}\ h^{-1}$. La décharge de la rivière a un impact très local sur la capacité tampon de pH des eaux côtières du Saint-Laurent, avec un faible impact négatif au printemps et à l'été, puis un faible impact positif à l'automne. Au cours de sa décharge/son transit, les processus de production primaire et/ou métabolique dans l'estuaire de la rivière Kamouraska augmentent les concentrations de carbone inorganique dissout originalement transporté par la rivière. Les apports latéraux sont de $69,5 \pm 1,6$; $51,3 \pm 1,0$ et $71,4 \pm 3,5$ $kg\ C\ h^{-1}$ durant les mois de juillet, août et octobre respectivement. Cette étude met en évidence la nécessité de quantifier des flux de carbone dans l'océan côtier, en mettant l'accent sur la connectivité continent-océan, et la saisonnalité des apports continentaux.

Mots clés : Flux de CO_2, Processus du carbone, Paramètres du système des carbonates, Décharge de rivière, Bilan carbone, Océan côtier

ABSTRACT

Gas exchange across the air-water interface is governed by Henry's law, and the capacity of the global ocean to uptake CO_2 is now well documented. In contrast, the characteristics of the coastal ocean as a net sink or source of CO_2 remain poorly constrained and are still debated. The coastal ocean is a dynamic environment regarding the production and consumption of dissolved inorganic carbon (DIC) and total alkalinity (TA), that, in turn, influences the pH buffering capacity and CO_2 exchange. The general objective of this study is to monitor the seasonal distribution of carbonate system parameters along a river – coastal ocean continuum. More specifically, the objectives were to 1) determine whether lateral inputs from a river and its estuary function as a sink or source of CO_2 to the atmosphere, 2) ascertain whether river discharge increases or decreases the pH buffering capacity of coastal waters, and 3) construct a seasonal carbon budget along the river – coastal ocean continuum. The Kamouraska River in the western Bas-Saint-Laurent (Quebec, Canada) region was chosen as a model for a small tributary of the Upper St. Lawrence Estuary (USLE). Surface waters were sampled along the salinity gradient from the river to the USLE, and carbonate system parameters (pH, TA, DIC, and partial pressure of CO_2) were measured in May, July, August, and October 2022, during the ice-free season. CO_2 fluxes to the atmosphere ranged from 94 ± 68 to 958 ± 238 μmol m^{-2} h^{-1}. River discharge has a very local impact on the pH buffering capacity of the coastal waters of the USLE, showing a small negative effect in the spring and summer, followed by a small positive effect in the fall. During outflow, primary and/or metabolic production processes in the Kamouraska River Estuary increase the concentrations of DIC originally transported by the river. Lateral inputs were 69,5 ± 1,6; 51,3 ± 1,0 and 71,4 ± 3,5 kg C h^{-1} in July, August, and October, respectively. This study emphasizes the need for further estimates of carbon fluxes in the coastal ocean, particularly focusing on the continent-ocean connectivity and seasonality of the terrestrial inputs.

Keywords: CO_2 fluxes, Carbon processes, Carbonate system parameters, River discharge, Carbon budget, Coastal Ocean

TABLE DES MATIÈRES

LISTE DES TABLEAUX

LISTE DES FIGURES

LISTE DES ABBRÉVIATIONS

Ω_{Ar}	État de saturation de l'eau par rapport à l'aragonite (*saturation state of aragonite*)
Ω_{Ca}	État de saturation de l'eau par rapport à la calcite (*saturation state of calcite*)
C	Carbone (*carbon*)
Ca	Calcium
$CaCO_3$	Carbonate de calcium (*calcium carbonate*)
CO_2	Dioxyde de carbone (*carbon dioxyde*)
CO_3^{2-}	Ion carbonate (*carbonate ion*)
CO2SYS	Programme de spéciation de la chimie du CO_2 (*CO_2-chemical speciation program)*
CTD	Conductivité-température-profondeur (*conductivity-temperature-depth*)
D	Décharge (*discharge*)
δC^{13}-DIC	Signature en C^{13} du DIC (*^{13}C signature of the DIC*)
DIC	Carbone inorganique dissout (*dissolved inorganic carbon*)
DOM	Matière organique dissoute (*dissolved organic matter*)
DSi	Silice dissoute (*dissolved silicate*)
ΣNO_3	Nitrates totaux (*total nitrates*)
F	Flux de CO_2 à l'interface air-eau (*CO_2 flux at the air-water interface*)
H^+	Ion hydrogène (*hydrogen ion*)
HCA	Analyse hiérarchique des grappes (*hierarchical clustering analysis*)
HCO_3^-	Ion bicarbonate (*bicarbonate ion*)
H_2CO_3	Acide carbonique (*carbonic acid*)

H_3O^+	Ion hydronium (*hydronium ion*)
KR-USLE	Rivière Kamouraska – estuaire supérieur du Saint-Laurent (*Kamouraska River – Upper St. Lawrence Estuary*)
LOAC	Continuum aquatique terre-océan (*land-ocean aquatic continuum*)
LOD	Limite de détection (*limit of detection*)
N	Azote (*nitrogen*)
NEC	Calcification nette de l'écosystème (*net ecosystem calcification*)
NEP	Production nette de l'écosystème (*net ecosystem production*)
NO_3	Nitrates
OrgAlk	Alcalinité organique (*organic alkalinity*)
P	Phosphore (*phosphorus*)
PC	Composante principale (*principal componant*)
PCA	Analyse en composantes principales (*principal component analysis*)
***p*CO_2**	Pression partielle de CO_2 (*CO_2 partial pressure*)
pH_T	pH sur l'échelle de concentration totale (*pH on the total concentration scale*)
POM	Matière organique particulaire (*particulate organic matter*)
S_P	Salinité pratique (*practical salinity*)
SRP	Phosphore réactif soluble (*soluble reactive phosphorus*)
T	Température (*temperature*)
TA	Alcalinité totale (*total alkalinity*)
USLE	Estuaire supérieur du Saint-Laurent (*Upper St. Lawrence Estuary*)

INTRODUCTION GÉNÉRALE

S'adapter aux changements globaux fait actuellement partie des défis majeurs auxquels nos sociétés doivent faire face. Il est donc aujourd'hui primordial d'approfondir nos connaissances des mécanismes et sources responsables de ces changements. Le dioxyde de carbone (CO_2) d'origine anthropique est le principal responsable de ces changements globaux, représentant plus de 75% des émissions de gaz à effet de serre (IPCC 2014), menant à une hausse de la concentration atmosphérique de CO_2 d'environ 40% depuis le début de l'ère industrielle (Zeebe 2012). Ces concentrations moyennes à l'échelle planétaire dépassent maintenant 400 ppm, et atteignent la concentration la plus élevée jamais enregistrée sur Terre depuis les trois derniers millions d'années (Willeit et al. 2019). L'océan global est le plus grand puits de CO_2 atmosphérique et a séquestré approximativement le tiers de tout le CO_2 émis par l'activité anthropique (Gruber et al. 2019, Gruber et al. 2009, Keeling and Manning 2014, Zeebe 2012), limitant jusqu'à présent l'augmentation observée des concentrations de CO_2 atmosphérique (Feely et al. 2004, Sabine et al. 2004). Cependant, cette capacité de puits de carbone implique des répercussions sur les processus physico-chimiques océaniques et de ce fait sur les écosystèmes marins par la détérioration de leur structure, de leur résilience, de leurs fonctions, ainsi que de leur biodiversité (Boyd et al. 2018, IPCC 2022).

Néanmoins, le caractère de puits ou de source nette de l'océan côtier à l'atmosphère est actuellement débattu, spécifiquement dû aux importantes variabilités spatiales, saisonnières et annuelles (Dai et al. 2022). Le budget global du carbone océanique ne tient pas compte de la mosaïque des processus naturels qui transforment, séquestrent ou produisent du carbone tout au long du continuum aquatique terre-océan, puisqu'il est basé principalement sur l'océan ouvert (Cai 2011, Cole et al. 2007, Regnier et al. 2013, Regnier et al. 2022). Ces derniers sont pourtant des facteurs majeurs de la dynamique de la chimie des carbonates dans les zones côtières (Bauer et al. 2013, Bourgeois et al. 2016, Regnier et

al. 2013). C'est pourquoi l'inclusion des zones côtières dans le cycle global du carbone et dans les budgets de l'océan global est encore aujourd'hui limitée. Quantifier les bilans de carbone régionaux est nécessaire afin d'approfondir notre connaissance de la dynamique de la chimie des carbonates des eaux côtières et plus précisément évaluer la capacité totale de l'océan à absorber les concentrations en CO_2 atmosphérique en constante augmentation.

FLUX DE CARBONE DE L'OCÉAN CÔTIER

Bien que les échanges gazeux à l'interface air-eau de l'océan global soient bien documentés, le caractère de puits ou de source nette de CO_2 de l'océan côtier est toujours peu contraint et sujet à débats (Borges et al. 2005, Cai and Dai 2004, Cai et al. 2006, Chen and Borges 2009, Dai et al. 2013, Laruelle et al. 2014, Roobaert et al. 2019, Thomas et al. 2004). Les estimations globales du flux annuel net de CO_2 de l'océan côtier à l'atmosphère varient de -0,19 à -0,45 Pg C y^{-1} avec une densité de flux variant de -6,0 à -12,0 g C m^{-2} y^{-1} (Borges et al. 2005, Cai et al. 2006, Chen et al. 2013, Dai et al. 2013, Laruelle et al. 2014), où les flux négatifs correspondent à un transfert de CO_2 de l'atmosphère vers les eaux de surface. Ces estimations sont des valeurs moyennes représentant de larges superficies. Elles offrent une résolution spatiale et temporelle limitée, considérant l'hétérogénéité de l'océan côtier (Roobaert et al. 2019), où les variations du comportement entre un puits et une source de CO_2 y sont les plus importantes (Cai et al. 2020) (Figure 1). Ces patrons de variabilité des flux nets de CO_2 rendent la tâche difficile pour catégoriser les différentes régions de l'océan côtier comme des puits ou des sources de CO_2, ainsi que de quantifier ces flux (Cai et al. 2020, Guo et al. 2015, Li et al. 2020). Le nombre limité d'observations *in situ* des flux côtiers de CO_2 à l'interface air-eau (Roobaert et al. 2022), ainsi que le comportement complexe du système des carbonates (système tampon principal du pH) tout au long du continuum continent-océan (Bauer et al. 2013, Regnier et al. 2022), contribuent à l'explication des larges incertitudes associées aux estimations des flux nets de CO_2 de l'océan côtier.

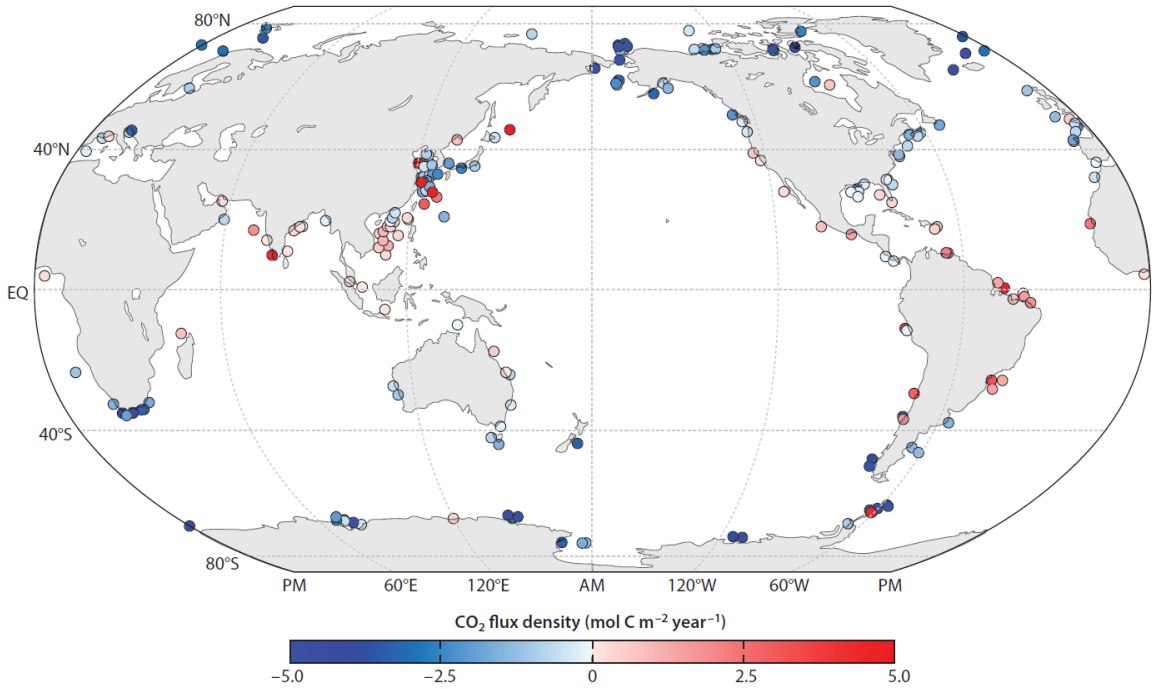

Figure 1. Localisation et estimations des flux de CO_2 à l'interface air-eau dans l'océan côtier global (ici, océan côtier est défini comme la marge océanique ou la marge continentale, voir la Figure 3). Le gradient de couleur réfère aux flux de CO_2 (en mol C m^{-2} an^{-1}). Les points en bleu rapportent des flux négatifs, soit des puits de carbone, alors que les points en rouge signalent des flux positifs, soit des sources de carbone à l'atmosphère. Tiré de Dai et al. (2022).

PARAMÈTRES DES CARBONATES

Afin d'estimer des flux nets de CO_2, il faut tout d'abord déterminer le gradient de la pCO_2 à l'interface air-eau directement ou selon une caractérisation des autres paramètres des carbonates. Quatre paramètres sont couramment mesurés, soit la pression partielle de CO_2 (pCO_2), le carbone inorganique dissout (DIC pour *dissolved inorganic carbon*), l'alcalinité totale (TA pour *total alkalinity*) et le pH. La pCO_2 dans l'eau est égale au ratio de la concentration actuelle sur la concentration à l'équilibre du dioxyde de carbone à une température, pression et salinité données, multiplié par la pCO_2 de la phase gazeuse ou dans l'atmosphère ($pCO_{2(atm)}$). La loi de Henry établit que la concentration d'un gaz à l'équilibre dans un liquide est directement proportionnelle à sa pression partielle au-dessus du liquide : $[CO_2]_{eq} = K_H \, pCO_{2(atm)}$; ainsi, plus la concentration atmosphérique est élevée, plus la

concentration dans la masse d'eau sous-jacente sera élevée. Lorsqu'il y a dissolution du CO_2 dans l'eau, une série de réactions a lieu selon les équations suivantes :

$$CO_2(g) \leftrightharpoons CO_2(aq) \quad \text{[Éq.1]}$$

$$CO_2(aq) + H_2O(l) \leftrightharpoons H_2CO_3(aq) \quad \text{[Éq.2]}$$

$$H_2CO_3(aq) \leftrightharpoons H^+(aq) + HCO_3^-(aq) \quad \text{[Éq.3]}$$

$$HCO_3^-(aq) \leftrightharpoons H^+(aq) + CO_3^{2-}(aq) \quad \text{[Éq.4]}$$

Les équations 1 à 3 sont hypothétiques, puisqu'il est difficile de différencier le CO_2 (aq) du H_2CO_3 (aq). Ces espèces sont généralement combinées et identifiées comme CO_2*. Les réactions du dioxyde de carbone dissout (1 à 3) deviennent alors :

$$CO_2(g) \leftrightharpoons CO_2^*(aq) \quad \text{[Éq.5]}$$

$$CO_2^*(aq) + H_2O(l) \leftrightharpoons H^+(aq) + HCO_3^-(aq) \quad \text{[Éq.6]}$$

L'entièreté des espèces chimiques du DIC est donc constituée du dioxyde de carbone (CO_2), de l'acide carbonique (H_2CO_3), de l'ion bicarbonate (HCO_3^-) et de l'ion carbonate (CO_3^{2-}), soit :

$$DIC = [CO_2^*] + [HCO_3^-] + [CO_3^{2-}] \quad \text{[Éq.7]}$$

L'abondance relative des espèces chimiques du DIC est fonction du pH, tel que représenté par le diagramme de Bjerrum (Figure 2).

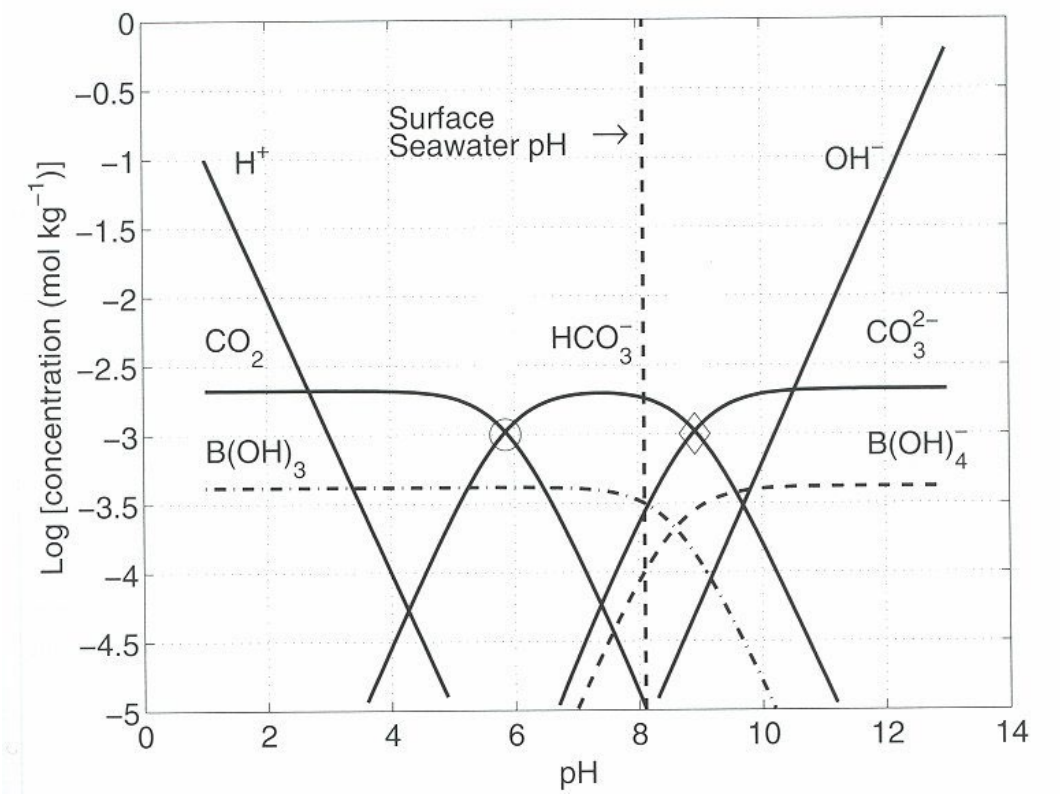

Figure 2. Diagramme de Bjerrum du système des carbonates, montrant les concentrations de HCO_3^-, CO_3^{2-} et le CO_2* (lignes pleines), ainsi que les concentrations de $B(OH)_3$ et $B(OH)_4^-$ (lignes pointillées) en fonction du pH (échelle totale) pour un DIC = 2,1 mmol kg^{-1}, une salinité = 35 et température = 25°C. Le cercle et le diamant indiquent le pK_1 = 5,86 et le pK_2 = 8,92 de l'acide carbonique, respectivement. Tiré de Zeebe et Wolf-Gladrow (2001).

Le DIC dans l'océan côtier provient de différentes sources. Les sources incluent le CO_2 atmosphérique, l'apport par les rivières, mais également la dégradation microbienne (ou reminéralisation) de la matière organique ou encore la dissolution de minéraux carbonatés dans la colonne d'eau ou les sédiments (Figure 3). La teneur en DIC peut être réduite par la photosynthèse (R1, Tableau 1), il peut être retourné à l'atmosphère, précipité sous forme de minéraux carbonatés, être exporté vers l'océan global ou être entreposé dans le sédiment (Regnier et al. 2022). La dégradation microbienne de la matière organique produit, en plus du CO_2 métabolique, des espèces réduites (voir Tableau 1) qui contribuent à l'alcalinité totale, lors de la respiration aérobie (R'1, Tableau 1), la réduction des nitrates (R2, Tableau 1) ou la réduction des sulfates (R3, Tableau 1).

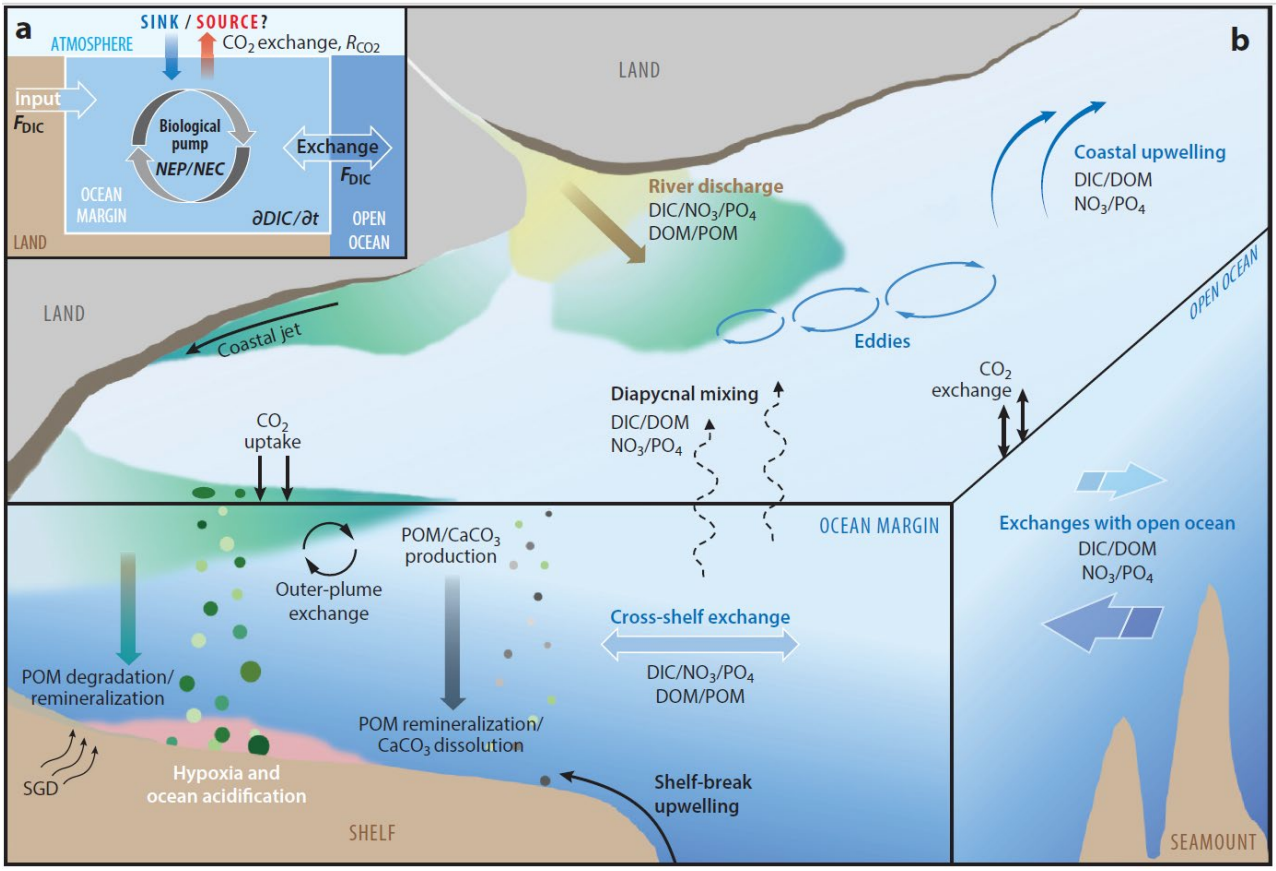

Figure 3. a) Schéma conceptuel simplifié des échanges de carbone inorganique dans le continuum terre-océan. b) Schéma conceptuel représentant les processus physiques et biogéochimiques dominants dans le continuum terre-océan. Les apports de rivière et des eaux souterraines sont représentés sur ce schéma, tout comme les échanges entre l'océan côtier et l'océan ouvert. Tiré de Dai et al. (2022). Abréviations : $CaCO_3$, carbonate de calcium ; DOM (pour *dissolved organic matter*), matière organique dissoute ; NEC (pour *net ecosystem calcification*), calcification nette de l'écosystème ; NEP (pour *net ecosystem production*), production nette de l'écosystème ; NO_3, nitrates ; PO_4, phosphates ; POM (pour *particulate organic matter*), matière organique particulaire.

Tableau 1. Sélection de réactions biogéochimiques et de la photosynthèse qui contribuent à la production/consommation de DIC et de TA.

Réactions individuelles	**ΔTA/ΔDIC**
(R1) Photosynthèse $106CO_2 + 122H_2O + 16HNO_3 + H_3PO_4 \rightarrow (CH_2O)_{106}(NH_3)_{16}H_3PO_4 + 138O_2$	+16/106 = 0,15
(R'1) Respiration aérobie $(CH_2O)_{106}(NH_3)_{16}H_3PO_4 + 138O_2 \rightarrow 106CO_2 + 122H_2O + 16HNO_3 + H_3PO_4$	-16/106 = -0,15 *
(R2) Réduction des nitrates $(CH_2O)_{106}(NH_3)_{16}H_3PO_4 + 84.8NO_3$ $\rightarrow 106CO_2 + 42.4N_2 + 16NH_3 + 148.4H_2O + H_3PO_4$	0,8/1 = 0,8
(R3) Réduction des sulfates $(CH_2O)_{106}(NH_3)_{16}H_3PO_4 + 53SO_4^{2-} + 166H^+$ $\rightarrow 106CO_2 + 106H_2O + 53H_2S + 16NH_3 + H_3PO_4$	1/1 = 1

R'1 provient de Chen and Wang (1999) (*). Il est à noter que la stœchiométrie de la matière organique est basée sur le rapport de Redfield C:N:P = 106/16/1.

L'alcalinité totale des eaux est définie de deux façons. Le concept de la balance de charges décrit l'alcalinité comme la somme des charges portées par les ions non conservatifs impliqués dans les réactions d'échange de protons en faisant abstraction des cations et des anions conservatifs dont la spéciation est indépendante du pH (Middelburg et al. 2020). L'alcalinité de titrage, connue comme la TA, décrit plutôt l'alcalinité comme la somme des bases qui sont titrables par un acide fort jusqu'au point d'équivalence correspondant à la conversion du bicarbonate en acide carbonique. Considérant que l'alcalinité a été mesurée par titrage dans cette étude, c'est cette dernière définition qui sera utilisée pour le reste de ce travail. La balance de protons de Dickson (1981) a été bonifiée afin d'inclure les acides forts (Soetaert et al. 2007, Wolf-Gladrow et al. 2007) ce qui résulte en une définition de la TA par cette équation :

$$TA = [HCO_3^-] + 2[CO_3^{2-}] + [B(OH)_4^-] + [OH^-] + [HPO_4^{2-}] + 2[PO_4^{3-}] + [H_3SiO_4^-] + 2[H_2SiO_4^{2-}] + [NH_3] + [HS^-] + 2[S^{2-}] - [H^+] - [HF] - [HSO_4^-] - 2[H_2SO_4] - [H_3PO_4] - [HNO_2] - [HNO_3] \quad \text{[Éq.8]}$$

L'alcalinité totale tamponne l'acidité produite par la dissolution du CO_2 dans l'eau (Éq.6) et l'effet tampon peut être représenté par le rapport TA/DIC. La capacité tampon est minimale lorsque les concentrations de TA et de DIC sont égales (rapport de 1) et augmente lorsque la valeur du rapport augmente (TA > DIC) ou diminue (TA < DIC) (Egleston et al. 2010). Cette capacité tampon limite l'impact de l'ajout d'un acide, tel le CO_2, sur le pH de la solution.

Selon la composition de la solution, il existe plusieurs échelles de pH afin de mesurer l'activité ou la concentration des ions hydrogène en solution. Dans le cadre de ce mémoire, l'échelle totale a été sélectionnée par son utilisation courante par les océanographes dans l'eau de mer. La concentration en ions hydrogène (H^+) est généralement représentée sur une échelle logarithmique via l'équation :

$$pH = -\log [H^+] \qquad \text{[Éq.8]}$$

Les ions hydrogène complètement libres n'existent qu'en petite proportion en solution, ils sont généralement complexés à une ou plusieurs molécules d'eau et sont généralement représentés par l'ion hydronium (H_3O^+). Ils peuvent également se complexer à d'autres composés pouvant influencer la détermination du pH, dont les ions sulfates (SO_4^{2-}) via l'équation suivante :

$$HSO_4^- \leftrightharpoons H^+ + SO_4^{2-} \qquad \text{[Éq.9]}$$

Les paramètres du système des carbonates peuvent être calculés à partir d'au moins deux des quatre paramètres mesurés. Les paires de paramètres les plus utilisées sont pH-TA et TA-DIC, puisque la mesure de ces paramètres est plus commune. Lorsque la TA est utilisée pour les calculs, les valeurs estimées de DIC et de pression partielle de CO_2 (pCO_2) peuvent être imprécises (Abril et al. 2015, Delaigue et al. 2020, Hunt et al. 2011, Song et al. 2020), plus particulièrement dans les eaux douces et côtières riches en matière organique. Les eaux côtières sont un lieu de décharge des eaux continentales riches en matière organique dissoute qui contribue positivement ou négativement à la TA (Abril and Borges 2005, Abril et al. 2000, Delaigue et al. 2020, Hunt et al. 2011). Cette contribution à la TA a un impact sur les

valeurs des paramètres des carbonates calculés à partir de la TA. Une surdétermination du système des carbonates (3 ou 4 des 4 paramètres) et la mesure *in situ* de la pCO_2 permettent d'obtenir des données directes et précises.

CONTINUUM AQUATIQUE TERRE-OCÉAN

L'océan côtier et, plus largement, l'ensemble du continuum aquatique terre-océan (LOAC pour *land-ocean aquatic continuum*) ne fait pas qu'échanger du CO_2 avec l'atmosphère, mais transporte et transforme du carbone tout au long du parcours (Borges et al. 2005, Cai et al. 2006, Cole et al. 2007, Meybeck 1982, Regnier et al. 2013, Regnier et al. 2022). Le LOAC est hautement dynamique : l'activité photosynthétique, la reminéralisation de la matière organique pélagique et benthique produit et/ou consomme du carbone inorganique dissout et de l'alcalinité totale. Ces derniers, à leur tour, contrôlent la capacité tampon de l'eau, les échanges de CO_2 à l'interface air-eau et les échanges de carbone avec l'océan ouvert (Bauer et al. 2013, Cai et al. 2011, Chen and Borges 2009, Dai et al. 2022, Hofmann et al. 2011, Lacroix et al. 2021) (Figure 3).

Cependant, la compréhension quantitative des échanges entre les différentes composantes du continuum rivière – eau côtière ainsi qu'avec l'atmosphère et du sort des différentes formes de carbone tout au long du continuum est pour le moment incomplet. La couverture limitée des observations, ainsi que la synergie entre les processus physiques (hydrologiques et géomorphologiques) et biogéochimiques (photosynthèse/respiration, la quantité et stœchiométrie des apports de matière organique) caractérisent la forte hétérogénéité des systèmes côtiers. L'étude de cas à une échelle spatiale et temporelle plus fine permet d'identifier les processus intervenant tout au long du continuum, passant d'une vision passive du LOAC à une compréhension mécanistique des processus qui y interviennent (Cole et al. 2007, Regnier et al. 2022) (Figure 4).

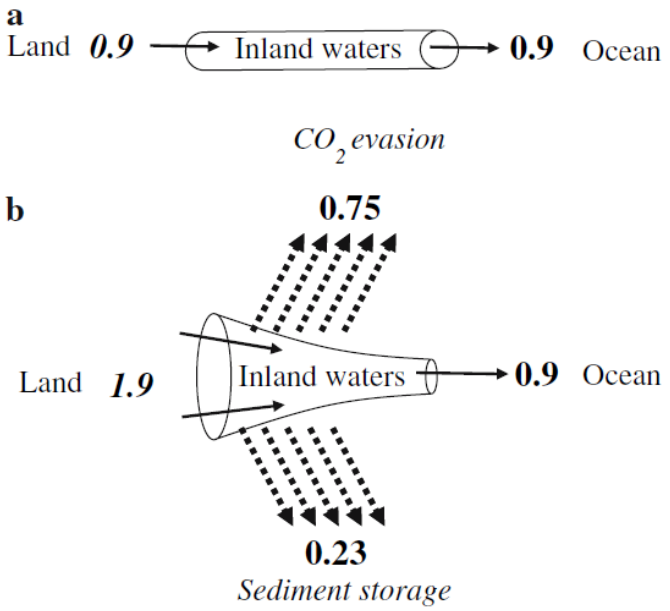

Figure 4. Schéma simplifié du rôle des eaux continentales dans le cycle global du carbone. a) Présentation d'un point de vue où les eaux continentales agissent comme un pipeline passif. Ainsi, le flux de 0,9 Pg C yr^{-1} transite du continent vers l'océan sans aucune transformation. b) Présentation d'un point de vue alternatif où les processus biogéochimiques qui opèrent lors du transport des eaux continentales modifient le cycle global du carbone. L'export continental est plus important (1,9 Pg C yr^{-1}) mais subit des transformations qui implique un échange de carbone avec le sédiment (perte par enfouissement de 0,23 Pg C yr^{-1}) et avec l'atmosphère (perte par dégazage de 0,75 Pg C yr^{-1}), avant de se déverser dans l'océan. Ici, le carbone est présenté comme étant accumulé dans le sédiment et émis vers l'atmosphère, mais peut aussi être émis par le sédiment à la suite de la diagénèse et être absorbé par les plans d'eaux. Tiré de Cole et al. (2007).

CONTEXTE DE LA ZONE D'ÉTUDE

La région du Kamouraska est située sur la côte sud de l'estuaire supérieur du Saint-Laurent (USLE pour *Upper St. Lawrence Estuary*). L'étude s'est concentrée sur le continuum eau douce – eau côtière, de la rivière Kamouraska jusqu'à 4 km de la côte dans l'USLE, qui sera identifié comme le continuum KR-USLE (pour *Kamouraska River – Upper St. Lawrence Estuary*) (Figure 5). Le choix s'est porté sur ce système, car la rivière est navigable à marée haute, permettant ainsi de faire des mesures en bateau dans l'estuaire de ce système qui est à l'étude depuis 2018 et donc l'accès à des données permet de mieux interpréter les résultats obtenus par cette étude.

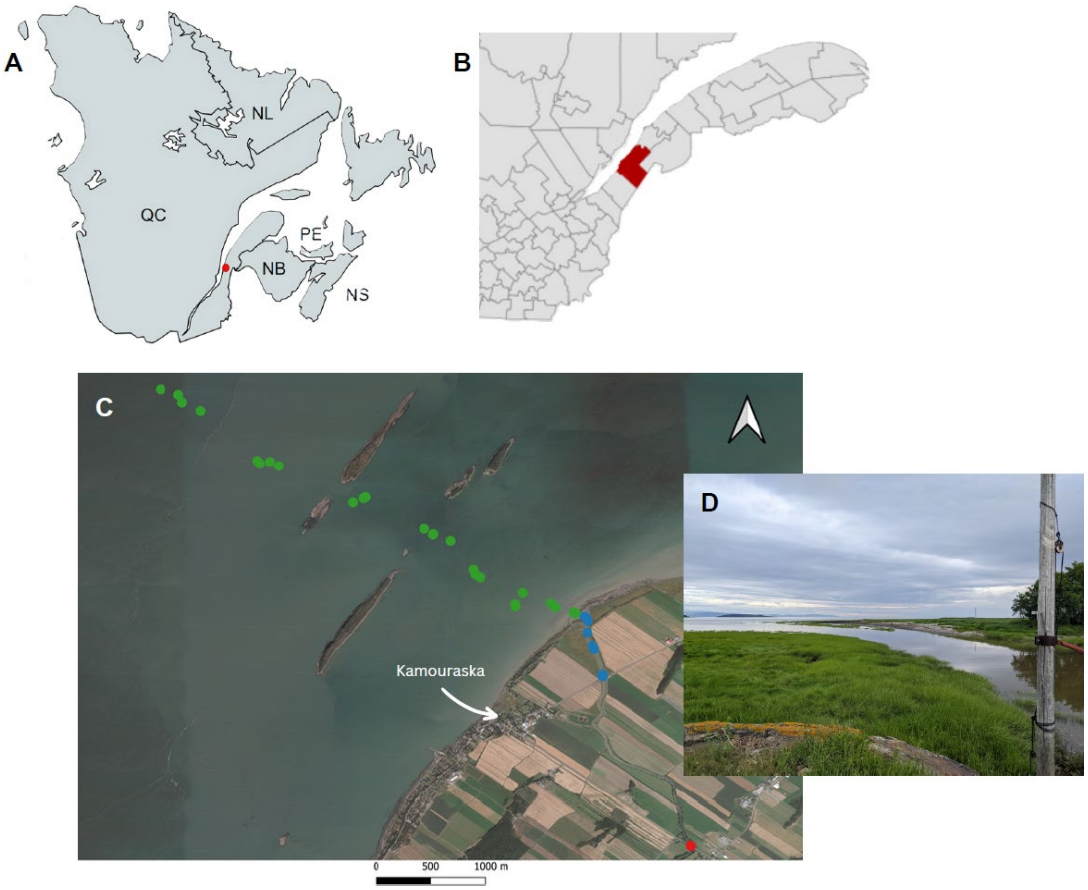

Figure 5. A) Localisation du continuum rivière Kamouraska – estuaire supérieur du Saint-Laurent sur une carte de l'est du Canada. B) Localisation de la région du Kamouraska au sein de l'est du Québec. C) Carte du site d'étude. Les points représentent les stations d'échantillonnage. Le point rouge représente la rivière Kamouraska, les points verts, l'estuaire supérieur du Saint-Laurent et les points bleus, l'embouchure de la rivière Kamouraska. D) Photo de l'embouchure de la rivière Kamouraska en juillet 2022.

La rivière Kamouraska draine un petit bassin versant (296 km^2), principalement forestier en amont (59%) et agricole, près de la côte, en aval (35%). La décharge de la rivière était de 3,98 m^3 s^{-1} en 2022, année de la campagne d'échantillonnage de cette étude. La décharge a atteint des valeurs aussi hautes que 9,04 m^3 s^{-1} durant la fonte des neiges au printemps, alors que le débit de base moyen est d'environ ~ 0,60 m^3 s^{-1} en hiver et été, soit les périodes d'étiage de faible débit (Gouvernement du Québec, Station hydrométrique 022601). La région des Appalaches, où se situe le continuum KR-USLE, est caractérisée par une roche mère composée de calcaire du Cambro-Ordovicien recouverte en amont par une fine couche de till et en aval par une épaisse couche d'argile déposée lors de l'inondation par

la mer de Goldthwait à la fin de la dernière glaciation (~ 20 à 11 ka). La zone côtière est caractérisée par une large zone intertidale de pente faible s'étendant jusqu'à 4 km de la côte, au large des Îles de Kamouraska, où la bathymétrie passe rapidement de 1,5 - 2 m à plus de 40 m de profondeur. Selon les données de la station marégraphique de Pêches et Océans Canada à Rivière-du-Loup, située à 20 km en amont de Kamouraska, les marées semi-diurnes dans cette zone montrent des marnages allant jusqu'à 3,0 mètres à marée de morte-eau et 5,6 mètres à marée de vive-eau. L'onde de marée se propage le long de la rivière Kamouraska jusqu'à environ 2,5 km en amont. L'intrusion d'eau salée dans la rivière, observée par des traits de sonde CTD (pour *conductivity– temperature – depth*) effectués en 2022, crée une stratification temporaire de la colonne d'eau : la couche supérieure est composée d'eau douce de la rivière qui s'écoule vers l'aval, indépendamment du cycle des marées, tandis que la couche inférieure est constituée d'eau salée, qui s'écoule vers l'amont ou l'aval dépendamment du cycle des marées.

Des études sur la dynamique des paramètres des carbonates ont été effectuées au travers du globe, mais seulement quelques-unes se sont intéressées en profondeur au LOAC d'une région spécifique (St-Laurent et al. 2020). Au Québec, la chimie des carbonates du LOAC a été étudiée par section, soit en rivière (Biehler et al. 2023, Campeau et al. 2014), dans le Fjord du Saguenay (Delaigue et al. 2020) ou dans l'estuaire du Saint-Laurent (Dinauer and Mucci 2017) et n'a pour le moment jamais été combiné à une étude de la saisonnalité. Notre étude serait donc la première à s'intéresser à la dynamique des paramètres des carbonates dans un continuum de ces secteurs, en procédant par leur mesure directe, ainsi qu'en s'intéressant à sa saisonnalité.

OBJECTIFS

Le continuum KR-USLE, en tant que zone côtière, représente une section du LOAC toujours peu représentée dans la littérature, comparativement à d'autres systèmes, tels que les estuaires ou l'océan ouvert. Cette étude permettra d'approfondir la compréhension de **la dynamique des paramètres des carbonates du continuum rivière Kamouraska – estuaire supérieur du Saint-Laurent**. Plus spécifiquement, la recherche vise à :

1) **Déterminer si la rivière et l'estuaire de la rivière Kamouraska agissent comme puits ou source de CO_2 à l'atmosphère ;**
2) **Déterminer si la décharge de la rivière augmente ou diminue la capacité tampon de pH des eaux côtières ;**
3) **Estimer et proposer un budget carbone le long du continuum rivière – océan côtier.**

CONTRIBUTION DE L'AUTEUR·E ET PUBLICATIONS

Le chapitre de ce mémoire est présenté sous forme d'article scientifique rédigé en anglais et intitulé « *Carbonate chemistry along a small river-coastal ocean continuum (Kamouraska River, Qc, Canada)* ». Cet article sera soumis prochainement à une revue scientifique avec comité d'évaluation de pairs.

Les données présentées dans le cadre de ce mémoire sont issues de quatre campagnes d'échantillonnage réalisées tout au long du continuum rivière Kamouraska – estuaire supérieur du Saint-Laurent en mai, juillet, août et octobre 2022. J'ai organisé et participé aux quatre campagnes de terrain. Les analyses de TA, DIC et pH ont été réalisées par Carole-Anne Guay et moi-même. Les échantillons de phosphore réactif dissout (SRP), de nitrates totaux (ΣNO_3) et de la silice dissoute (DSi) ont été réalisés par Pascal Rioux et moi-même à l'Institut des Sciences de la Mer de Rimouski. Les analyses de δC^{13}-DIC ont été réalisées par

Jean-François Hélie et moi-même au Laboratoire de géochimie des isotopes stables légers à l'Université du Québec à Montréal (GEOTOP-UQÀM, Montréal, QC, Canada). Les données sont toutes accessibles sur le site de l'Observatoire global du Saint-Laurent (OGSL).

CHAPITRE 1
CHIMIE DES CARBONATES LE LONG D'UN PETIT CONTINUUM RIVIÈRE-OCÉAN CÔTIER (KAMOURASKA, QC, CANADA)

RÉSUMÉ EN FRANÇAIS DU PREMIER ARTICLE

Depuis le début de l'ère industrielle, les émissions anthropiques de dioxyde de carbone (CO_2) ont augmenté la concentration de CO_2 dans l'atmosphère de la Terre jusqu'à atteindre des niveaux records sur les trois derniers millions d'années. Le CO_2 émis à l'atmosphère est redistribué dans différents réservoirs, incluant les océans. En raison des échanges gazeux à l'interface air-océan, ces derniers ont absorbé approximativement le tiers du CO_2 émis par les activités humaines, limitant son accumulation dans l'atmosphère et les changements climatiques globaux. Bien que la séquestration de carbone par l'océan global soit maintenant bien documentée et a mené à l'acidification des océans, le caractère de source/puits net de carbone de l'océan côtier est toujours mal contraint et sujet à débats. L'océan côtier est un environnement hautement dynamique, où les processus biogéochimiques incluant la photosynthèse et la reminéralisation benthique et pélagique (respiration microbienne) de la matière organique, ainsi que la calcification biogène et la dissolution de minéraux carbonatés produisent et/ou réduisent les teneurs en carbone inorganique et alcalinité totale qui, à leur tour, influencent la capacité tampon du pH de l'eau et les échanges de CO_2 avec l'atmosphère. L'intensité de ces processus varient grandement dans le temps et l'espace, ce qui engendre une grande hétérogénéité des flux nets de CO_2. La quantification des échanges et du devenir des différentes formes du carbone tout au long du continuum rivière – océan côtier demeure incomplète, à cause du nombre limité de données ainsi que de l'hétérogénéité physique (hydrologique et géomorphologique) et biogéochimique (magnitude et stœchiométrie des apports en matière organique) des systèmes côtiers. Dans cette étude, une analyse des paramètres de la chimie du carbone inorganique

dissout a été effectuée le long d'un continuum allant de la rivière Kamouraska, jusqu'à l'estuaire supérieur du Saint-Laurent, où la rivière se décharge. Plus spécifiquement, les trois principaux objectifs de l'étude étaient de : 1) déterminer si le continuum agit comme un puits ou une source de CO_2 à l'atmosphère ; 2) déterminer si la décharge de la rivière augmente ou diminue la capacité tampon du pH des eaux côtières ; et 3) quantifier un budget du carbone inorganique du continuum rivière-océan côtier. L'estimation des flux de carbone démontre que les eaux de surface agissent comme une source de CO_2 à l'atmosphère lors de la période de l'étude, avec des valeurs allant de 94 (± 68) à 958 (± 238) μmol m^{-2} h^{-1} pour l'ensemble du continuum. Le suivi du rapport TA/DIC suggère une faible influence acidifiante de la rivière sur les eaux côtières au printemps et à l'été, alors que cette influence est plutôt alcaline en automne. L'élaboration d'un budget du carbone inorganique a permis d'estimer la décharge en carbone inorganique dissout à l'estuaire supérieur, avec des valeurs allant de 49,0 (± 0,9) à 123,0 (± 13,0) kg C h^{-1}, ainsi que de l'alcalinité totale, avec des valeurs allant de 3,96 (± 0,11) à 10,2 (± 0,4) $\times 10^3$ mol h^{-1}. Ce budget montre aussi que les processus benthiques participent à la production et remobilisation de carbone inorganique le long du continuum, contribuant à la production de 12% à 37% du carbone inorganique exporté aux eaux côtières. Les résultats de cette étude soulignent non seulement la contribution significative des apports latéraux sur la chimie des eaux côtières mais aussi leurs grandes variabilités saisonnières. Ils mettent en évidence la nécessité de disposer d'estimations supplémentaires des flux de carbone dans l'océan côtier, en mettant l'accent sur la connectivité terrestre, ainsi que sur la saisonnalité des apports.

Ce premier chapitre, rédigé sous le format d'un article scientifique intitulé « Carbonate chemistry along a small river-coastal ocean continuum (Kamouraska, Qc, Canada) » a été rédigé par moi-même et révisé par les professeur·es Gwénaëlle Chaillou, Fanny Noisette et Alfonso Mucci. Il a aussi bénéficié des commentaires des deux évaluateurs de ce mémoire.

Les résultats de cette maîtrise ont été présentés lors de congrès sous la forme de présentations orales ou par affiche et les données ont été publiées, comme indiqué ci-dessous :

Présentations par affiche :

Olivier Turcotte, Charles-Édouard Deschamps, Fanny Noisette, Alfonso Mucci, Gwénaëlle Chaillou, Dynamique de la chimie des carbonates dans les eaux côtières du Kamouraska, 31 janvier – 3 février 2022, RSA de Québec-Océan 2022, en ligne.

Olivier Turcotte, Carole-Anne Guay, Fanny Noisette, Alfonso Mucci, Gwénaëlle Chaillou, Les eaux côtières sont-elles un puits ou une source de carbone à l'atmosphère ? Étude de cas de la rivière Kamouraska, 20-22 juin 2023, Congrès Avenir Maritime 2023, Québec (Québec, Canada).

Présentation orale :

Olivier Turcotte, Carole-Anne Guay et Gwénaëlle Chaillou, Dynamique du carbone inorganique dissout dans la zone de mélange d'un affluent du Saint-Laurent, 6-7 février 2023, RSA de Québec-Océan 2023, Rivière-du-Loup (Québec, Canada).

Données publiées :

Turcotte, O., Guay, C.-A., Mucci, A., Noisette, F., & Chaillou, G. (2025). *Carbonate Chemistry Along a Small River-Coastal Ocean Continuum (Kamouraska River, Qc, Canada)* [Data set]. https://doi.org/10.26071/cf2735e1-e4e2-4dbd

CARBONATE CHEMISTRY ALONG A SMALL RIVER-COASTAL OCEAN CONTINUUM (KAMOURASKA RIVER, QC, CANADA)

Olivier Turcotte[1], Alfonso Mucci[2], Fanny Noisette[1] and Gwénaëlle Chaillou[1]

[1] Québec-Océan and Institut des Sciences de la Mer de Rimouski, Université du Québec à Rimouski, 310 Allée des Ursulines, Rimouski, Québec G5L 3A1, Canada
[2] GEOTOP and Department of Earth and Planetary Sciences, McGill University, 3450 University Street, Montreal, Québec H3A 0E8, Canada

Correspondence: Olivier Turcotte (olivier.turcotte@uqar.ca)

INTRODUCTION

Since the beginning of the industrial era, anthropogenic emissions of carbon dioxide (CO_2) have increased the concentration of CO_2 in the Earth's atmosphere by around 40% (Zeebe and Ridgwell 2011), to more than 400 ppm, an unprecedented level over at least the past 3 million years (Willeit et al. 2019). The CO_2 emitted to the atmosphere is redistributed into various reservoirs including the ocean. As a result of gas exchange across the air-sea interface, the latter has absorbed approximately one-third of the CO_2 emitted by human activities (Gruber et al. 2019, Gruber et al. 2009, Keeling and Manning 2014, Zeebe and Ridgwell 2011). Without this oceanic uptake, the atmospheric CO_2 partial pressure would be about 55 ppm higher than currently observed (Sabine et al. 2004), mitigating, in part, climate change.

Whereas gas exchange across the air-sea interface is dictated by Henry's law and the global ocean CO_2 uptake and consequent ocean acidification are well documented, the net carbon dioxide source/sink characteristics of the coastal ocean are still poorly constrained and debated (Borges et al. 2005, Cai and Dai 2004, Cai et al. 2006, Chen and Borges 2009, Dai et al. 2013, Laruelle et al. 2014, Roobaert et al. 2019, Thomas et al. 2004). The coastal ocean is a highly dynamic area where biogeochemical processes, including photosynthesis, benthic and pelagic organic matter remineralization (microbial respiration), and biogenic calcification, as well as carbonate mineral dissolution produce and/or consume both dissolved inorganic carbon (DIC) and total alkalinity (TA) (Bauer et al. 2013, Cai 2011, Chen

and Borges 2009, Dai et al. 2022, Hofmann et al. 2011, Lacroix et al. 2021). In turn, the latter control the pH buffering capacity and air-sea CO_2 exchanges of the receiving waters. The estimated global, annual net air-sea CO_2 flux of the coastal ocean ranges from −0,19 to −0,45 Pg C y^{-1} with the majority of fluxes being between −0,5 and −1,0 mol C m^{-2} y^{-1} (Borges et al. 2005, Cai et al. 2006, Chen et al. 2013, Dai et al. 2013, Dai et al. 2022, Laruelle et al. 2014), the negative fluxes corresponding to a CO_2 transfer from the atmosphere to the sea surface. Coastal ocean regions show extensive spatial and temporal net CO_2 fluxes heterogeneity, and many are known to alternate between carbon sinks and sources depending on the season, weather, and time of the day (Cai et al. 2020, Roobaert et al. 2019). These net CO_2 flux patterns make it difficult to categorize the coastal ocean as a net source or sink of CO_2 and to quantify these fluxes at a larger scale (Cai et al. 2020, Guo et al. 2015, Li et al. 2020). The limited number of *in situ* observations of coastal air-sea CO_2 fluxes (Roobaert et al. 2022) and the complex behavior of carbonate system parameters, including the DIC, pH, and TA, along the land-coastal ocean continuum (Bauer et al. 2013, Regnier et al. 2022), explain the large uncertainties on estimates of the net coastal ocean CO_2 fluxes and mis-estimates the contribution of coastal ocean to global ocean carbon budget.

Concerns about the long-term fate of CO_2 in the oceans have motivated scientists to examine the distributions of DIC and TA (Feely et al. 2004), but technical and logistical challenges have impeded widespread surveys. The carbonate system parameters can be computed from two of the four readily measured parameters (pH, TA, DIC, and pCO_2), most commonly pH and TA or TA and DIC. When TA is used for calculations, computed pCO_2 and DIC values can be inaccurate, especially in organic-rich freshwater and coastal waters where the contribution of organic alkalinity (OrgAlk) is often neglected in the calculation but can be positive or negative (Abril et al. 2015, Delaigue et al. 2020, Hunt et al. 2011, Song et al. 2020). An overdetermination of the carbonate system (3 or 4 of the 4 parameters) and *in situ* measurements of the pCO_2 can circumvent this problem, but they are more challenging to acquire due to the additional sampling logistics and more elaborate analytical procedures. A quantitative understanding of the exchange and fate of different forms of carbon along the river-to-coastal ocean continuum is so far incomplete, owing to limited data coverage and

the physical (e.g., hydrological and geomorphological) and biogeochemical (e.g., primary productivity, respiration and the stoichiometry of organic matter inputs) heterogeneity of coastal subsystems. In this study, an analysis of carbonate system parameters was carried out during the ice-free season of 2022 along the Kamouraska River on the southern shore of the Upper St. Lawrence Estuary (USLE). More specifically, the objectives were to determine whether the river and the mixing zone serve as a source or sink of atmospheric CO_2, and if the river discharge increases or decreases the pH buffering capacity of the coastal waters. Finally, the results of this study allow for the elaboration of a quantitative carbon budget along the continuum.

METHODS

1.1 Study site

This study was conducted in the Kamouraska region on the south shore of the USLE (Figure 6). The research focused on a freshwater–coastal water continuum, from the Kamouraska River up to 4 km from the coastline within the estuary, that will, thereafter, be identified as the Kamouraska River - Upper St. Lawrence Estuary (KR-USLE) continuum. The Kamouraska River drains a small (296 km^2) catchment that is mainly forested (59%) upstream and agricultural (35%) downstream near the coastline. Its mean annual freshwater discharge was 3,98 m^3 s^{-1} in 2022. The bankfull discharge reaches as high as 9,04 m^3 s^{-1} during the spring snowmelt in May, whereas the mean baseflow discharge is about ~ 0,60 m^3 s^{-1} during the winter and summer low-flow periods (Government of Quebec, Hydrometric station 022601). In this Appalachian Mountain region, the bedrock catchment is composed of Cambro-Ordovician limestones covered by a thin till layer upstream and by a thick clay layer downstream, that was deposited during the Goldthwait Sea flood at the end of the last glaciation. The coastline is characterized by a large intertidal muddy flat extending 4 km offshore to the Kamouraska Islands (Figure 6B) where the bathymetry drops from 1,5 to 2,0 m to > 40 m depth. According to the Fisheries and Oceans Canada Rivière-du-Loup climate station (https://marees.gc.ca/fr/stations/03130) located about 20 km downstream, this area is

characterized by semi-diurnal tides ranging from 3,0 m at neap tide to 5,6 m during spring tide. The tide propagates along the riverbed, nearly 2,5 km upstream within the Kamouraska River.

1.2 Sampling

The data presented in this study were collected on four (4) distinct sampling campaigns during the ice-free season of 2022, in May, July, August, and October. These periods were chosen because they differ in terms of hydroclimatic conditions (from bankfull to base flow discharges, as described above) and marine productivity (minimum of 0,88 mg m^{-3} of chlorophyll α, in May, and maximum of 5,9 mg m^{-3} of chlorophyll α, in July (Julliard et al. 2023), in the nearshore zone. During each sampling campaign, 10 to 13 stations located from upstream of the river mouth to 4 km offshore were visited (Figure 6C). Our sampling strategy was to sail and collect samples from the river to the USLE during the high-sea slack tide (that lasts ~1 hour after the high tide) to limit the effect of tide wave propagation during the sampling period. From a small boat, water was continuously drawn from 0,5 to 1,0 m below the water surface using a submersible pump deployed over the side and injected at a rate of ~30 L min^{-1} into a spray chamber secured onboard. The water depth and position of the boat were continuously recorded by a DualBeam sonar (200 kHz and 83 kHz) and GPS Chartplotting. After 15 minutes of pre-equilibration, the equilibrated air was continuously pumped from the spray chamber through a Drierite desiccant before being channelled to a LI-830 (LICOR) CO_2 analyzer. The LI-830 probe operates through the rapid diffusion of gases through a supported semipermeable membrane to a thermostated cell (> 50 °C) in which the CO_2 mole fraction of the gas is quantified by a nondispersive infrared detector. The probe was operated in continuous mode, with measurements at each second in August and October, every 10 seconds in May, and every 30 seconds in July (3% measurement error based on the manufacturer's specifications). The boat moved slowly (~5 km h^{-1} to limit air bubble contamination) between each station where discrete sampling was carried out. Each *in situ* pCO_2 measurement was then coupled to a GPS location. The temperature (T) and

practical salinity (S_P) were measured throughout the water column using a manufacturer-calibrated Sea-Bird SBE19plus conductivity – temperature – depth (CTD) probe deployed from the boat. Concomitantly, a 6L-Niskin bottle was deployed from the side of the boat to collect surface water (between 0,5 and 1,0 m below the surface). The surface water samples were transferred directly from the Niskin bottle into 500 mL borosilicate bottles for later analyses of DIC, δC^{13}-DIC, and $TA_{(meas)}$. Each bottle was flushed three (3) times before being filled without headspace, poisoned with 100 µL of a saturated mercuric chloride ($HgCl_2$) solution and tightly sealed with a Teflon stopper that was secured by cramping of an aluminum cap. The samples were stored in the dark at room temperature. For the total pH (pH_T) determinations, 125 mL plastic bottles were filled without headspace and put on ice until analysis within the following 8 hours. Falcon tubes were filled with 12 mL of 0,2 µm (cellulose acetate membrane) filtered water for the soluble reactive phosphorus (SRP), total nitrate ($\Sigma NO_3 = NO_3 + NO_2$), and dissolved silica (DSi) analyses. These samples were kept on ice until stored at -80 °C upon returning to the laboratory until thawed for the analyses.

As the upstream river station was not accessible by boat, it was sampled from shore, except in May because of technical problems. A daily-calibrated (with manufacturer-supplied solutions) multi-parametric probe (YSI 600QS) was used to measure T and S_P. A submersible pump was deployed a few decimeters below the surface to avoid any air bubble contamination, and the water was sampled and stored in the same manner as described above.

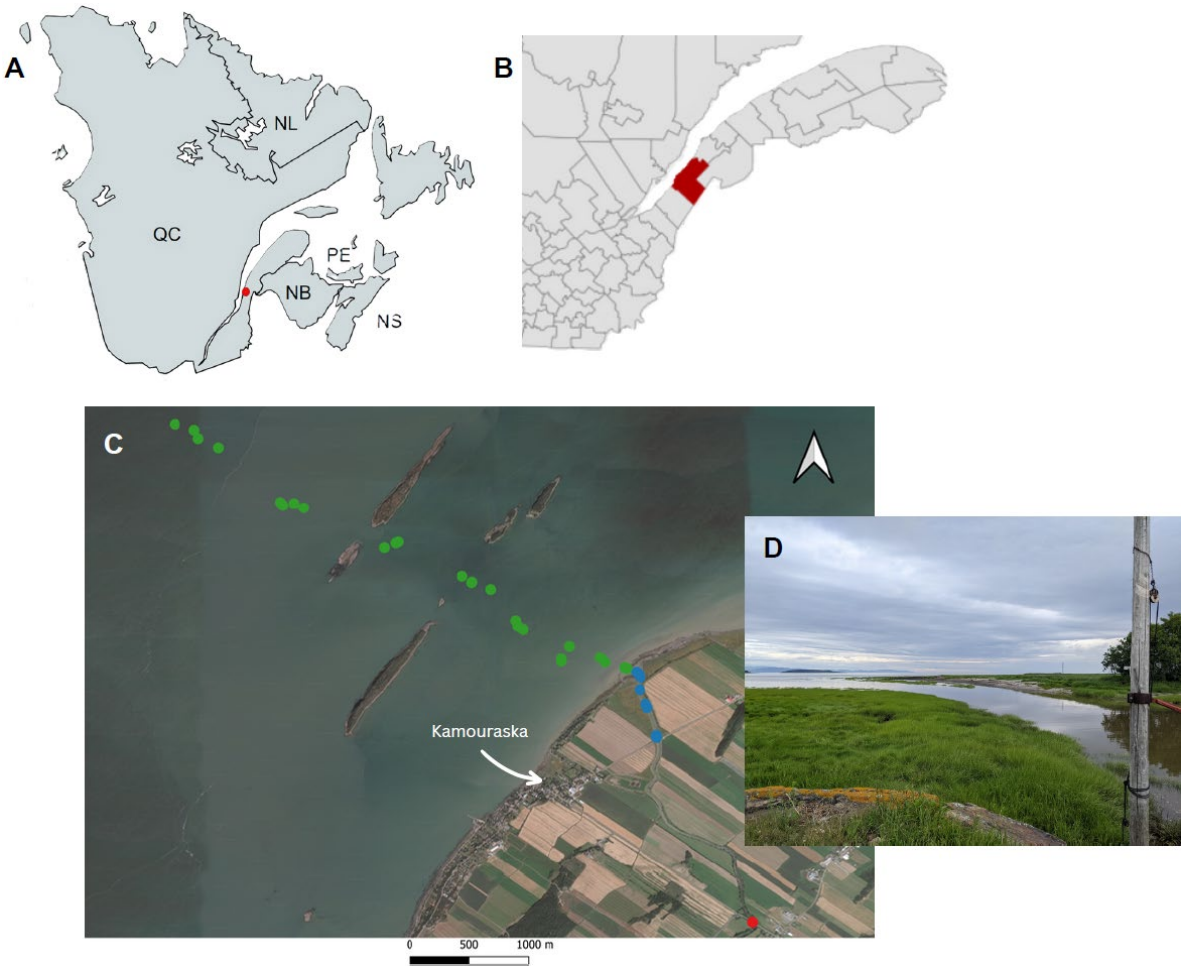

Figure 6. A) Location of the Kamouraska River to the Upper St. Lawrence Estuary continuum on a map of Eastern Canada provinces. B) Location of the Kamouraska region within Eastern Québec. C) Map of the study site, Kamouraska River to the Upper St. Lawrence Estuary continuum, Qc, Canada. The dots represent the location of the sampling stations. The red, blue, and green colors represent zones 1, 2, and 3 as distinguished by the HCA (see section Results for a detailed explanation). D) Picture of the Kamouraska River transition zone to the coastal waters of the Upper St. Lawrence Estuary, taken in July 2022.

1.3 Other chemical parameters

The dissolved inorganic carbon (DIC) was determined on an Apollo SciTech Multi-Sample Analyzer (AS-C6L) system at the Université du Québec à Rimouski (UQÀR). After thermally equilibrating the system at 25°C, 3 mL of the sample was injected into the instrument's reactor, where it was acidified with 3% H_3PO_4 and the evolved CO_2 was carried by a continuous stream of helium to a LI-COR infrared analyzer. A calibration curve was constructed using gravimetrically prepared Na_2CO_3 solutions, and the accuracy of the

measurements was verified using certified reference material (CRM, batch 72) solutions provided by Andrew Dickson's lab (Scripps Institute of Oceanography). The reproducibility of the measurements on replicate analyses of the same sample was, on average, 0,11%. $TA_{(meas)}$ was measured using an automatic titrator (Metrohm 848 Titrino plus) with a pH electrode (Metrohm, 6.0262.100). The HCl titrant prepared in distilled water was calibrated using certified reference materials (CRM, batch 72). The average reproducibility of the measurements on replicate analyses of the same standard was 0,50%. It is important to note that the $TA_{(meas)}$ may also include a contribution from organic alkalinity (Cai et al. 1998).

The total pH (pH_T) was determined spectrophotometrically on the total hydrogen ion concentration scale, using phenol red and unpurified m-cresol purple as indicators and a Hewlett-Packard UV-visible diode array spectrophotometer (HP-8453A) with a 5 cm quartz cell. Samples (125 mL plastic bottles) were thermally equilibrated in a constant temperature bath at 25 °C before all readings. The salinity-dependence of the dissociation constants and molar absorptivities of the indicators were taken from Robert-Baldo et al. (1985) for phenol red and from Douglas and Byrne (2017) for m-cresol purple. The reproducibility of the pH_T measurements was determined on replicate analyses of the same sample and was, on average, ± 0,005.

The ^{13}C signature of the DIC ($\delta^{13}C$-DIC) samples was analyzed at the Light Stable Isotope Geochemistry Laboratory at Université du Québec à Montréal (UQÀM) using a Micromass MicroGasTM system coupled to an Isoprime 100TM Isotope Ratio Mass Spectrometer (IRMS) in continuous flow mode. Carbon isotopic values are reported in per mil (‰) with respect to Vienna PeeDee Belemnite (VPDB) referenced to the NBS-19 and LSVEC scale. Two internal reference materials ($\delta^{13}C$ = -3,41 ± 0,06‰ and -19,51 ± 0,05‰ vs VPDB) were used to normalize the results on the NBS19-LSVEC scale. The overall analytical uncertainty is better than ± 0,1‰.

Nutrients (SRP, ΣNO_3, and DSi) samples were analyzed on an Automatic Analyser AA500 (Seal Analytical) at UQÀR. A calibration curve was constructed for each nutrient

using suitably diluted, gravimetrically-prepared stock solutions. The limits of detection (LOD) were determined to be 0,02, 0,18, and 0,30 µM for the SRP, ΣNO_3, and DSi, respectively, as three times the standard deviation of a low concentration standard run ten times. The reproducibility of the measurements was estimated at 3,9%, 2,1%, and 0,2%, respectively, for the SRP, ΣNO_3, and DSi, based on replicate analyses of the same samples. These values were exclusively used as inputs in the CO_2-chemical speciation program (CO2SYS) to enhance the robustness of the calculations.

1.3.1 Calculated parameters

Dissolved inorganic carbon (DIC), SRP, and DSi concentrations as well as pH_T were used as input parameters in CO2SYS (Excel v.3.0_Err, Pierrot et al. 2021) to compute the calculated TA ($TA_{(calc)}$), CO_2 partial pressure ($pCO_{2(calc)}$), and saturation states of the waters with respect to the two most common calcium carbonate polymorphs, aragonite ($\mathbf{\Omega}_{Ar}$) and calcite ($\mathbf{\Omega}_{Ca}$). The carbonic acid dissociation constants (K_1 and K_2) of Cai and Wang (1998), the HSO_4 dissociation constant taken from Dickson (1990), the HF dissociation constant of Perez and Fraga (1987), and the total borate concentration: S_P ratio of Lee et al. (2010) were used for the calculations. The carbonic acid dissociation constants of Cai and Wang (1998) were selected because they return calculated pCO_2 ($pCO_{2(calc)}$) values that are closest to the measured values, particularly in low salinity waters (Dinauer and Mucci 2017). The saturation states of freshwater with respect to the carbonate polymorphs were computed using PHREECQ and the calcium (Ca) concentrations of the Kamouraska River in 2021, taken from the "Atlas de l'eau" (Government of Quebec, Station 02260002). The saturation states of the brackish and seawater were calculated from Ca concentrations computed by CO2SYS from S_P and corrected for Ca concentration derived on a conservative mixing line.

To confirm the quality of the measured carbonate system parameters, they were also calculated with the CO2SYS program using a combination of the former. The TA-pH_T pair was used to calculate the DIC and $pCO_{2(calc)}$, the DIC-pH_T pair was used to calculate the TA, and the $TA_{(meas)}$-DIC parameter combination was used to calculate the pH_T, in combination

with the SRP and DSi concentrations to overdetermine the system. The consistency between the measured and calculated parameters was better than 2,2%, with the largest differences being for the calculated pCO_2 (as high as 2,15%). Table 2 presents the cumulative error calculated using the CO2SYS program for each calculated parameter for samples collected in August 2022. The errors were in the same range for the other sampling campaigns.

Table 2. Average error of the calculated carbonate system parameters in August 2022, using the CO2SYS program.

Month	Station	DIC (%)	TA (%)	pH_T (%)	pCO_2 (%)
August	1	0.58	0.14	0.46	1.48
	2	0.50	0.12	0.80	1.54
	3	0.48	0.11	0.80	1.58
	4	0.47	0.11	0.80	1.63
	5	0.41	0.11	0.39	1.74
	6	0.43	0.12	0.39	1.98
	7	0.43	0.12	0.39	2.00
	8	0.43	0.13	0.38	2.02
	9	0.43	0.12	0.39	2.15
	10	0.43	0.12	0.39	2.11

1.4 Statistics

Statistical analysis was used to regroup the sampling stations based on their chemical parameters to improve our interpretation and better integrate their spatial and temporal variability. A Principal Component Analysis (PCA) was performed on the entire database using the chemical parameters that were not auto-correlated ($R^2 < 0,95$), as determined using the *chart.correlation* function in RStudio. S_P, T, pH_T, DIC, SRP, ΣNO_3, and DSi were selected, and the database was centred on further analyses using the *deconstand* function. The eigen-values for each principal component (PCs) were extracted and the Euclidean method was used to create a distance matrix whereas hierarchical clustering analysis (HCA) was applied using Ward's linkage method. The elbow method was used to determine the

number of clusters in the dataset. All statistical analyses were carried out with RStudio (version 4.2.2, R Core Team, 2022).

1.5 CO_2 fluxes at the air-water interface

Based on the HCA results, clusters were defined and used to delineate zones within which CO_2 fluxes at the air-water interface were calculated for each sampling period. Each zone is constituted of the samples included in the zone and the mean value of the different parameters (DIC and $TA_{(meas)}$) was used for subsequent flux calculations (see below). Since tides influence the direction of lateral transport between each zone, the sampling was carried out at high-sea slack tide, and the lateral transport between each zone was assumed to be only driven by the river discharge.

The CO_2 air-water fluxes were estimated using the method described in Wanninkhof (2014), according to the following equation (1) :

$$FCO_2 = k * K_0(pCO_2w - pCO_2a) \quad (1)$$

where F is the CO_2 flux at the air-water interface (mol m^{-2} y^{-1}), k is the gas transfer velocity (m y^{-1}), K_0 is the CO_2 solubility (mol l^{-1}), and pCO_2w and pCO_2a (ppm or µatm) are, respectively, the partial pressures of CO_2 in the surface water and the overlying air. k was calculated using the Wanninkhof (2014) equation (2) :

$$k = 0{,}251 < U10^2 > (\frac{Sc}{660})^{-0{,}5} \quad (2)$$

where $<U10^2>$ is the average squared wind speed (m s^{-1}) measured at 10 meters above the water surface and Sc is the Schmidt number for CO_2 at a given temperature. The $U10$ was estimated using the hourly wind speed data taken from the Rivière-Du-Loup meteorological station operated by the Environment and Climate Change Canada - Meteorological Service of Canada (Station 7056616). The parameters used for the F calculations are reported in Table 4. The pCO_2a was assumed to be 420 ppm, the average global atmospheric

concentration of 2022, based on measurements carried out at the Mauna Loa Observatory operated by the National Oceanic and Atmospheric Administration (NOAA).

Each measured pCO_2 value ($pCO_{2(meas)}$) was associated with a temperature and S_P, to compute *F* values. An average *F* value, calculated from all measurements within each zone, was then calculated. The values of *F* are presented in µmol m^{-2} h^{-1} and not in a per-year unit because the data represent instantaneous snapshots that are not representative of the whole spatial and temporal variability within the KR-USLE continuum. The positive values of *F* indicate the release of CO_2 to the atmosphere by surface waters, whereas negative values imply that surface waters serve as a sink of atmospheric CO_2.

RESULTS

1.6 Physico-chemical properties along the salinity gradient

Three (3) groups of samples were identified by the HCA (hereafter referred to as zone 1, zone 2, and zone 3) and distributed along the KR-USLE continuum (Figure 6C). The geochemical features of each zone and season are reported in Table 3. Zones 2 and 3 regroup significantly different samples (p-value < 0,19), except in May. Zone 1 was not statistically different from the other zones; zone 1 (in red in Figure 6C) only grouped the few samples collected upstream in the Kamouraska River. Thus, Zone 1 will be treated as the freshwater endmember of the KR-USLE continuum. Zone 1 was characterized by waters with S_P values close to 0, more depleted δC^{13}-DIC values, and a TA/DIC close to 1. In contrast, the zone 3 samples, regrouping the samples collected in the USLE (in green in Figure 6C), exhibited the highest salinities and their waters were enriched in δC^{13}-DIC. Zone 3 samples display similar properties (i.e., with low standard deviations) within and between sampling campaigns. The zone 2 samples, that regroup samples collected in the Kamouraska River Estuary (in blue in Figure 6C), exhibited the most variable properties, with very high S_P and pH_T variability between sampling campaigns.

The practical salinity (S_P) along the KR-USLE continuum ranged from 0 to 24 in the first meter below the air-water interface and reached S_P higher than 25 below 5 m depth

(Figure 7A). In May and July, the water column was highly stratified in the seaward section of the continuum and towards the USLE. The surface waters of the Kamouraska River Estuary were mainly composed of fresh to brackish waters ($0 < S_P < 10$). In August and October, the water column was more homogeneous in the seaward section. The water column in the Kamouraska River Estuary, however, was more stratified, with freshwater limited to the first meter below the surface. The temperatures ranged from 1 to 18 °C and exhibited an opposite distribution to the S_P. Surface water temperatures in the Kamouraska River Estuary were always higher than in the USLE, reaching > 15 °C during the summer (July and August), whereas the surface temperatures were around 10-12 °C in the USLE. In October, the surface temperatures dropped to < 8 °C in the Kamouraska River Estuary and were around 6 °C in the USLE.

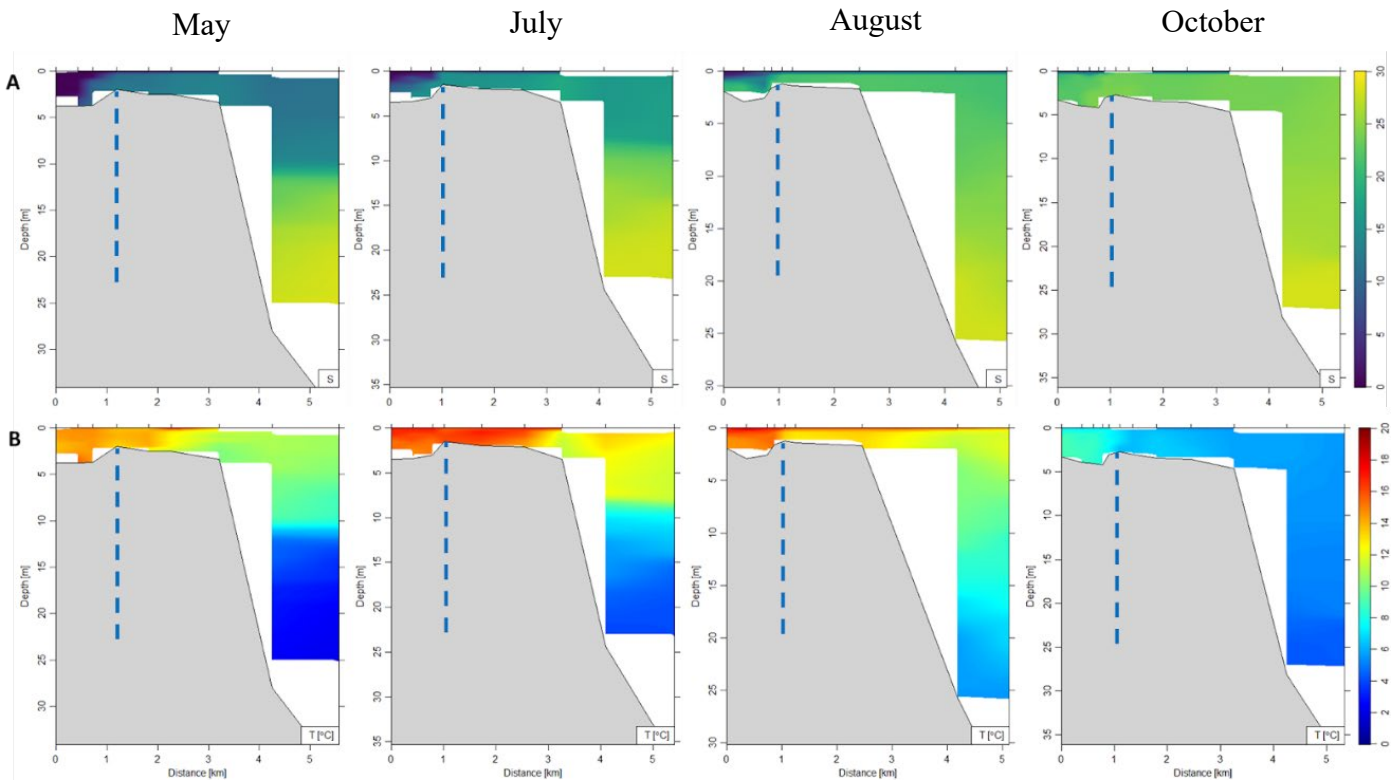

Figure 7. Vertical sections of practical salinity, S_P (A), and temperature, T (°C) (B) along the Kamouraska River to the Upper St. Lawrence Estuary continuum for the sampling campaigns of May, July, August, and October 2022 during the high-sea slack tide. An interpolation was applied between field data points in R Studio, using the "oce" package. The blue dashed line represents the boundary between zones 2 and 3, as revealed by the HCA (see text for details). The 0 km point represents the most upstream station attainable by boat, that excludes from the Figure the river endmember station for each month.

1.7 Accuracy of the measured and calculated carbonate system parameters

Given that up to four of the readily measurable carbonate system parameters were measured at each sampling in this study, the self-consistency and accuracy of the measurements could be verified. The correlation between $TA_{(meas)}$ and $TA_{(calc)}$ (from DIC-pH_T) (Figure 8) reveals a discrepancy, with $TA_{(meas)}$ exceeding $TA_{(calc)}$. The absolute discrepancy increases progressively with salinity but shows a larger variability in freshwater (S_P = 0,0 to 0,2) (average of 4,6%). This implies that species not accounted for in the $TA_{(calc)}$ computations (carbonate, boric, phosphoric, and silicate alkalinity were accounted for) contribute to $TA_{(meas)}$. The most likely contribution would be from organic alkalinity (OrgAlk). In fresh and brackish waters, where dissolved organic matter concentrations are

typically higher, the non-carbonate and non-borate fractions of TA can make up a significant fraction of the TA. Similar contribution of OrgAlk to TA, up to > 3%, were measured in other coastal waters (Kuliński et al. 2014, Song et al. 2020). Likewise there appears to be a significant contribution of OrgAlk to $TA_{(meas)}$ in the KR-USLE continuum. Thus, when $TA_{(meas)}$ is used as an input parameter in speciation calculations, these will yield doubtful values for other carbonate parameters, and slightly higher pCO_2 if OrgAlk is positive (Hunt et al. 2011, Kuliński et al. 2014). Dinauer and Mucci (2017) estimated that, at most, the error in the USLE was 1,9%. As noted by Abril et al. (2015), given the potential error introduced when using $TA_{(meas)}$ to calculate the pCO_2, the use of *in situ* pCO_2 is preferred for CO_2 flux calculations.

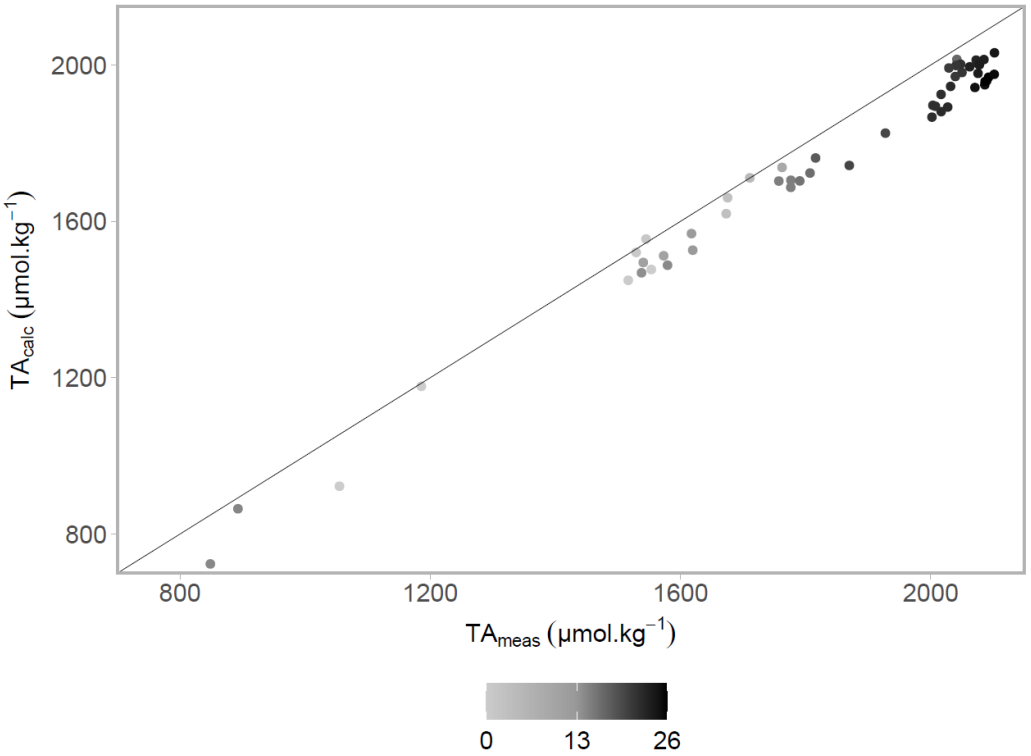

Figure 8. Calculated TA vs measured TA from all samples. The gray color scale represents the practical salinity of the samples. The black line is the 1:1 relationship.

1.8 Distribution and behaviors of the carbonate system parameters along the studied continuum

Overall, DIC concentrations in the surface waters ranged from 807 to 2009 µmol kg^{-1} (Figure 9A). The concentrations were lowest in May in zone 2 and reached 2009 µmol kg^{-1} in zone 3 during the August and October campaigns. TA concentrations varied between 849 and 2102 µmol kg^{-1} and paralleled those of DIC, with low $TA_{(meas)}$ in May in zone 2 and the highest values recorded in zone 3 during August and October. DIC and $TA_{(meas)}$ concentrations exhibited clear non-conservative mixing behavior along the continuum, suggesting that DIC and TA production occurs within the continuum. The pH_T behavior is more complex. The lowest value (pH_T = 6,9) was measured in zone 2 samples in May and the highest value was recorded in zone 1 in August (pH_T = 8,8). The variability of pH_T values was high throughout the continuum, whatever the sampling campaign, ranging from 6,9 to 8,0; 7,6 to 8,4; 7.5 to 8,8 and 7,4 to 8,4 in May, July, August, and October, respectively. The $\delta^{13}C$-DIC values ranged from -13,6 to 1,3 ‰. They were lowest in July in zone 1 and reached their highest value in October in zone 3. The $\mathbf{\Omega}_{Ca}$ and $\mathbf{\Omega}_{Ar}$ values ranged from 0,08 to 7,59 and 0,04 to 5,50, respectively. The values were lowest in October in zone 1 and highest in October in zone 2 (Table 3).

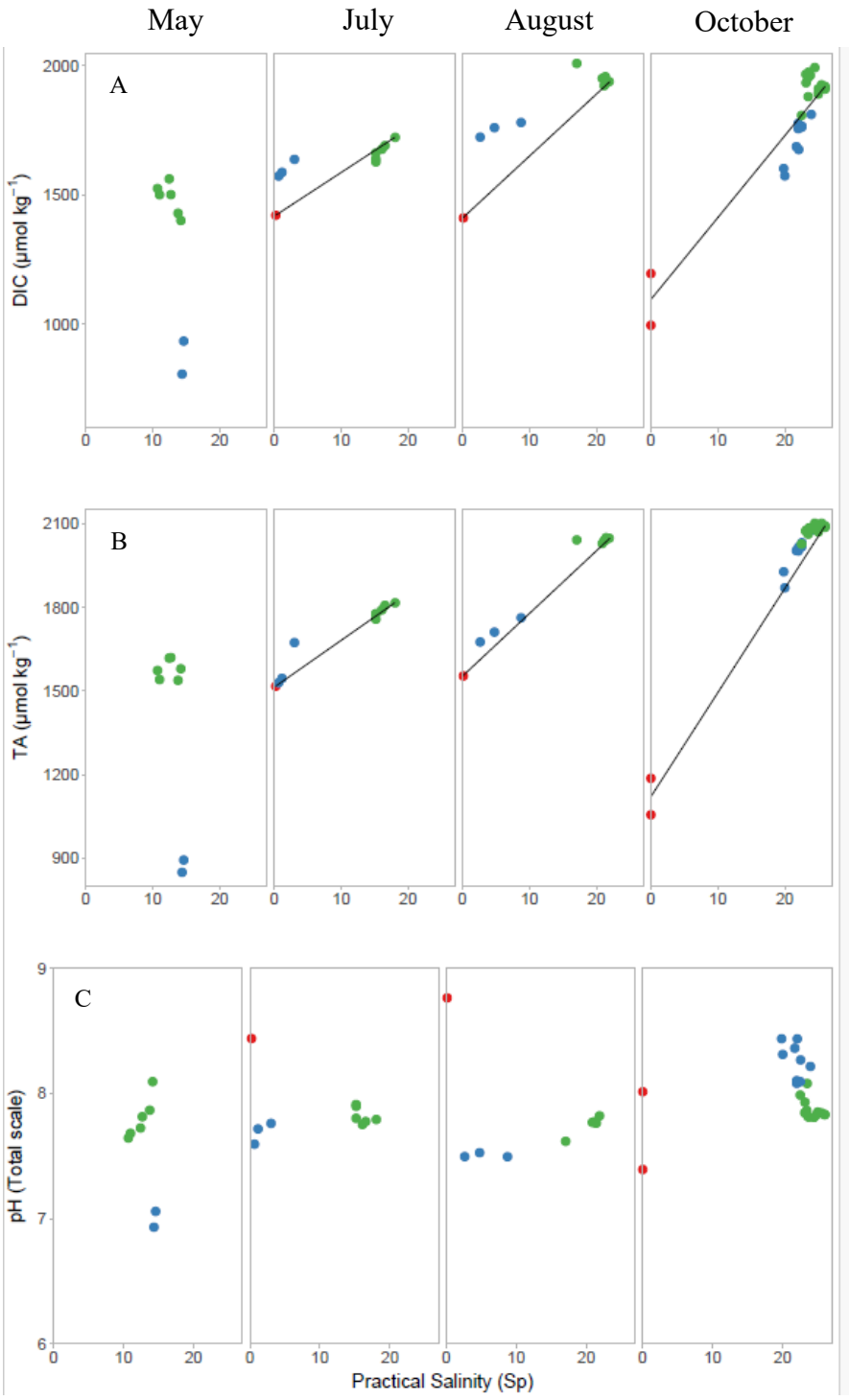

Figure 9. A) DIC, B) $TA_{(meas)}$, and C) pH_T vs practical salinity (S_P) for the samples taken in the months of May, July, August, and October 2022 (respectively represented from left to right) during the high-sea slack tide. The conservative mixing line (black line) between the freshwater and seawater endmembers is drawn for each variable using a salinity-based mixing model. For each sampling campaign, the river sample was considered the freshwater endmember, and the saltiest sample was considered the seawater endmember. The various colors represent the different zones associated with each group, as determined by the HCA: zone 1 is in red, zone 2 in blue, and zone 3 in green (see text for details).

Table 3. Mean and standard error of discrete sample measured (S_P, T, DIC, $TA_{(meas)}$, pH_T, δC^{13}-DIC) and calculated ($TA_{(calc)}$, $\mathbf{\Omega}_{Ca}$, $\mathbf{\Omega}_{Ar}$, TA/DIC) parameters along the continuum. Values are presented per zone and sampling month, where the n represents the number of sample.

May												
Zones	n	Sp	T (°C)	DIC (µmol kg^{-1})	$TA_{(meas)}$(µmol kg^{-1})	$TA_{(calc)}$(µmol kg^{-1})	pH_T	δ^{13}C-DIC (‰)	ΩCa	ΩAr	TA/DIC
1	*N/A*	*N/A*	*N/A*	*N/A*	*N/A*	*N/A*	*N/A*	*N/A*	*N/A*	*N/A*	*N/A*
2	14	14.48 ± 0.17	15.75 ± 0.35	871 ± 90	871 ± 31	794 ± 100	7.00 ± 0.09	-12.80 ± 1.13	0.10 ± 0.03	0.06 ± 0.02	1.00 ± 0.07
3	6	12.46 ± 1.41	13.75 ± 1.64	1488 ± 60	1578 ± 36	1510 ± 35	7.80 ± 0.16	-3.05 ± 0.37	1.06 ± 0.52	0.62 ± 0.31	1.06 ± 0.04
July											
Zones	n	Sp	T (°C)	DIC (µmol kg^{-1})	$TA_{(meas)}$(µmol kg^{-1})	$TA_{(calc)}$(µmol kg^{-1})	pH_T	δ^{13}C-DIC (‰)	ΩCa	ΩAr	TA/DIC
1	1	0.23	19	1422	1517	1449	8.44	-13.14	4.17	2.95	1.07
2	3	1.61 ± 1.24	17.47 ± 0.06	1600 ± 34	1582 ± 79	1565 ± 50	7.69 ± 0.09	-11.60 ± 2.43	0.46 ± 0.16	0.26 ± 0.09	0.99 ± 0.03
3	6	16.03 ± 1.15	15.65 ± 2.05	1670 ± 35	1787 ± 22	1714 ± 26	7.82 ± 0.07	-2.82 ± 1.50	1.41 ± 0.25	0.83 ± 0.15	1.07 ± 0.01
August											
Zones	n	Sp	T (°C)	DIC (µmol kg^{-1})	$TA_{(meas)}$(µmol kg^{-1})	$TA_{(calc)}$(µmol kg^{-1})	pH_T	δ^{13}C-DIC (‰)	ΩCa	ΩAr	TA/DIC
1	1	0.12	21.5	1411	1553	1477	8.76	-11.42	7.59	5.50	1.10
2	3	5.38 ± 3.10	16.26 ± 0.47	1755 ± 29	1716 ± 44	1703 ± 39	7.51 ± 0.02	-10.87 ± 0.65	0.47 ± 0.08	0.26 ± 0.05	0.98 ± 0.01
3	6	20.62 ± 1.78	13.02 ± 1.53	1952 ± 31	2041 ± 7	1993 ± 16	7.75 ± 0.07	-1.40 ± 1.06	1.45 ± 0.20	0.88 ± 0.13	1.05 ± 0.02
October											
Zones	n	Sp	T (°C)	DIC (µmol kg^{-1})	$TA_{(meas)}$(µmol kg^{-1})	$TA_{(calc)}$(µmol kg^{-1})	pH_T	δ^{13}C-DIC (‰)	ΩCa	ΩAr	TA/DIC
1	2	0.00 ± 0.00	10.00 ± 2.10	1096 ± 141	1120 ± 93	1050 ± 181	7.70 ± 0.44	-11.10 ± 0.14	1.66 ± 2.13	1.15 ± 1.47	1.03 ± 0.05
2	9	21.85 ± 1.27	10.00 ± 2.12	1713 ± 83	1995 ± 60	1884 ± 59	8.25 ± 0.14	-0.39 ± 0.35	3.38 ± 0.95	2.04 ± 0.57	1.17 ± 0.03
3	14	24.29 ± 1.13	5.54 ± 0.73	1924 ± 48	2079 ± 19	1979 ± 37	7.87 ± 0.08	-0.13 ± 0.43	1.62 ± 0.52	0.99 ± 0.32	1.09 ± 0.03

1.9 Surface-water pCO_2 along the continuum and CO_2 fluxes at the air-water interface

Large spatial variations in surface-water pCO_2 were measured along the continuum, with values ranging from 116 (± 22) ppm to 1669 (± 107) ppm in zones 1 and 2, respectively. Overall, the pCO_2 was higher in zone 2 than in zone 1 and 3. Larger pCO_2 gradients were observed along the continuum in May and October than in the summer months (July and August). Zone 2 and 3 pCO_2 values were higher in summer than in May and October, whereas zone 1 pCO_2 values were higher in October than in summer (Table 4, Figure 10). Large spatial variations in the air-water CO_2 fluxes were observed along the continuum, with fluxes varying from -228 µmol m^{-2} h^{-1} in zone 1 to 894 µmol m^{-2} h^{-1} in zone 2 in August (Table 4, Figure 10). The CO_2 fluxes, *F,* were almost always positive in zone 2 (20 to 894 µmol m^{-2} h^{-1}), with negative values only occurring in October. They were either negative or positive in zone 1 (- 228 to 169 µmol m^{-2} h^{-1}) and zone 3 (- 95 to 290 µmol m^{-2} h^{-1}).

Table 4. Means and standard errors of the pCO_2, $k660$, $U10$, and CO_2 fluxes (F) in the Kamouraska River to Upper St. Lawrence Estuary continuum. Values are presented per zone and sampling month. Note that the pCO_2 values correspond to *in situ* measurements.

May				
Zones	pCO_2 (ppm)	k 660 (cm h^{-1})	$u10$ (m s^{-1})	F (µmol m^{-2} h^{-1})
1	*N/A*	*N/A*	*N/A*	*N/A*
2	725 ± 12	2.07 ± 0.01	3.06	280 ± 11
3	463 ± 221	1.97 ± 0.09		40 ± 204

July				
Zones	pCO_2 (ppm)	k 660 (cm h^{-1})	$u10$ (m s^{-1})	F (µmol m^{-2} h^{-1})
1	161 ± 5	0.48 ± 0.00		-49 ± 1
2	1669 ± 107	0.45 ± 0.00	1.39	236 ± 20
3	584 ± 130	0.44 ± 0.02		31 ± 25

August				
Zones	pCO_2 (ppm)	k 660 (cm h^{-1})	$u10$ (m s^{-1})	F (µmol m^{-2} h^{-1})
1	116 ± 22	1.98 ± 0.01		-228 ± 16
2	1602 ± 39	1.80 ± 0.02	2.78	894 ± 29
3	802 ± 254	1.65 ± 0.06		290 ± 193

October				
Zones	pCO_2 (ppm)	k 660 (cm h^{-1})	$u10$ (m s^{-1})	F (µmol m^{-2} h^{-1})
1	763 ± 13	0.90 ± 0.00		169 ± 7
2	460 ± 86	0.93 ± 0.01	2.22	20 ± 43
3	227 ± 37	0.86 ± 0.02		-95 ± 18

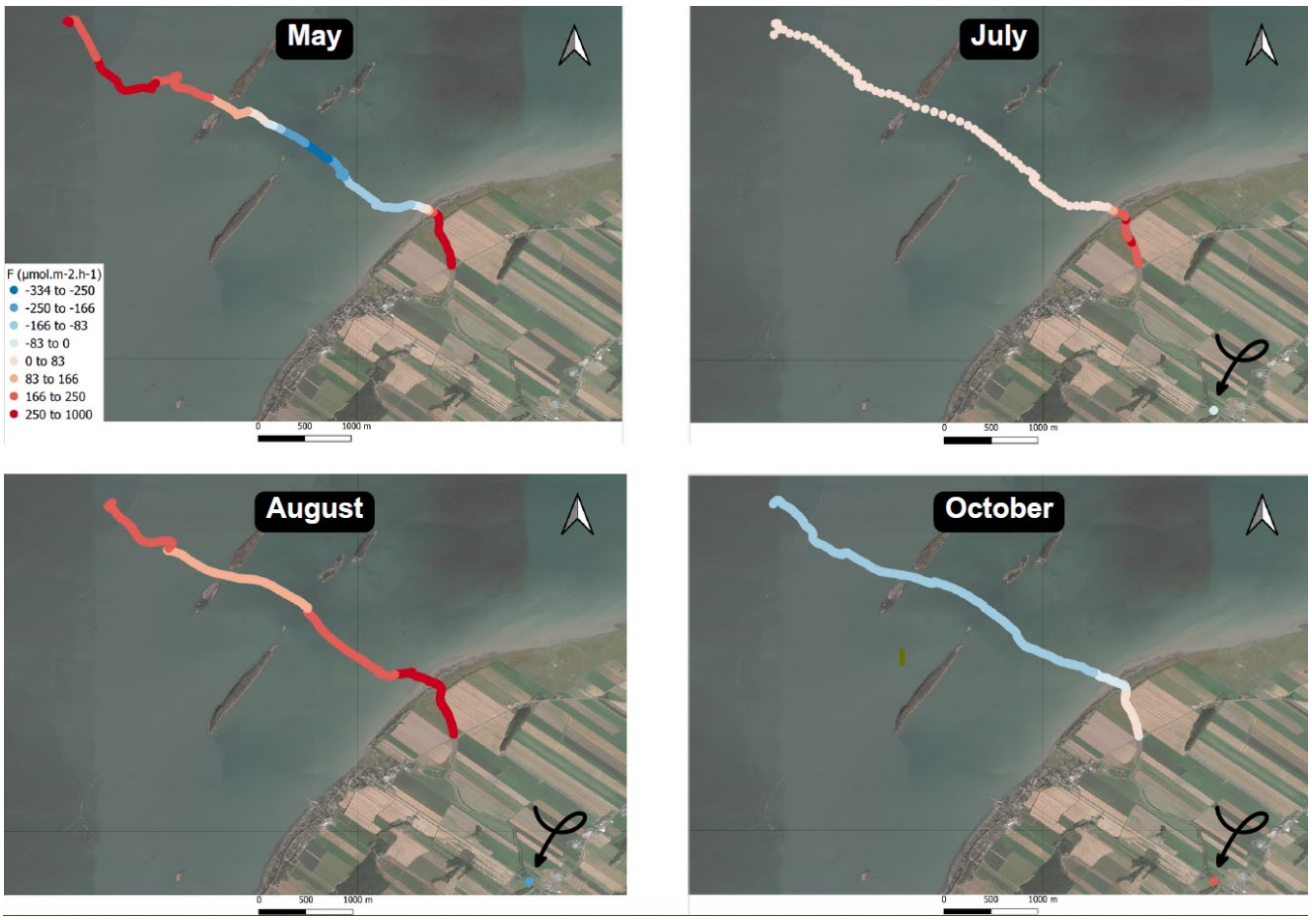

Figure 10. Spatial distribution of CO_2 fluxes (*F)* in the Kamouraska River to Upper St. Lawrence Estuary continuum during the high-sea slack tide, per sampling month. The curly arrow points to the location of the sampling station in the upstream part of the continuum. The gradient of colors represent the intensity and direction of the flux: negative fluxes (sinks), from the atmosphere to the surface water, in blue colors, and positive fluxes (sources), from the surface water to the atmosphere, in red colors.

DISCUSSION

1.10 LOAC waters as a source or sink of atmospheric CO_2?

The pCO_2 gradient across the air-sea interface is controlled by biological (photosynthesis and respiration), thermodynamic (solubility), and physical processes (mixing) that modulate changes in T, S_P, DIC, and TA (Abril et al. 2015, Borges 2005, Poisson et al. 1993). The CO_2 fluxes depend on the sea state (waves) that is most commonly parameterized as a function of the wind speed, and pCO_2 gradient. The KR-USLE was divided into three zones based on the HCA results. These zones act as either CO_2 sinks or

sources depending on the season (Figure 10). Whereas the offshore surface waters of the Kamouraska River Estuary (zone 2) were always a source of CO_2, the surface waters of the USLE (zone 3) were a lower CO_2 source in the summer and a CO_2 sink in the spring and fall periods. In contrast, upstream, the fresh section of the continuum (zone 1) was a sink of CO_2 in the summer and a source in October. From a compilation of 165 estuaries worldwide, almost all systems, with the exception for those in the Arctic (F = -1,1 mol C m^{-2} yr^{-1}, Chen et al., 2013), serve as sources of CO_2 to the atmosphere (Chen et al., 2013). Chen et al. (2013) concluded that most of the world's upper estuaries (S_P < 2) are strong sources (39,0 ± 55,7 mol C m^{-2} yr^{-1}), mid-estuaries (2 < S_P < 25) are moderate sources (17,5 ± 34,2 mol C m^{-2} yr^{-1}) and lower estuaries (S_P > 25) are weak sources of CO_2 (8,4 ± 14,3 mol C m^{-2} yr^{-1}). Within the LOAC, inland waters typically emit most of the CO_2 due to their high organic carbon content and higher rates of organic carbon respiration, but they also display the greatest variability in CO_2 fluxes (Bauer et al. 2013, Laruelle et al. 2015).

Since the bedrock catchment basin of our study area is rich in limestone, the groundwater DIC and TA concentrations are high in the region (~900 and ~1780 µmol kg^{-1}, respectively, Tommi-Morin et al. 2022). The groundwater DIC values are similar to those of the surface waters, over the spring period, of the Kamouraska River Estuary (871 µmol kg^{-1}) and lower than the USLE (1488 µmol kg^{-1}), whereas the TA values are slightly higher than the USLE (1578 µmol kg^{-1}) and higher than the Kamouraska River Estuary (871 µmol kg^{-1}). Our results reinforce the idea that groundwaters are an important contributor of the surface river waters in the Appalachian region, especially during the summer low-flow period, and they mostly contribute to determining the DIC/TA input (Biehler et al. 2023). Assuming that the lowest river discharge rate of ~0,20 m^3 s^{-1} corresponds to the persistent supply of groundwater to the Kamouraska River, we roughly estimate the groundwater contribution to be 6%, 20%, 31%, and 21% in May, July, August, and October, respectively.

In addition to these inputs, light conditions (intensity and period) and high water temperatures may favor the uptake of DIC by primary producers during daylight hours in the summer period and the shorter daylight hours and lower water temperature limit their proliferation and DIC uptake in October (Sournia 1975). The limited dataset in the river

section and the absence of nighttime measurements, however, limit the temporal extrapolation in terms of net fluxes.

Air-water CO_2 fluxes along the continuum were obtained by adding the CO_2 fluxes of the three zones throughout the KR-USLE continuum for each sampling campaign. The continuum is always observed to act as a global source of CO_2 to the atmosphere. The CO_2 fluxes ranged from 94 (± 68) to 958 (± 238) µmol m^{-2} h^{-1} (0,82 ± 0,60 to 8,39 ± 2,08 mol m^{-2} y^{-1}, 27,0 ± 19,6 to 276 ± 69 mg C m^{-2} d^{-1})[1], with minimum values in October and maxima in August. These values are comparable to those reported for rivers located in the Appalachian and Canadian Shield regions. For example, Biehler et al. (2023) measured CO_2 emissions of 88 to 529 mg C m^{-2} d^{-1} in the Matane River (Canada). In Abitibi and James Bay rivers (Canada), Campeau et al. (2014) determined a mean CO_2 flux of 449 mg C m^{-2} d^{-1} and, in the James Bay region, Teodoru et al. (2009) reported a mean CO_2 emission of 391 mg C m^{-2} d^{-1} from the Rivière à l'Eau Claire. Air-sea CO_2 fluxes in the USLE (zone 3, 0,7 ± 0,6 mmol m^{-2} d^{-1} or 8,4 ± 7,2 mg C m^{-2} d^{-1}) are lower but of the same order of magnitude as the flux estimates (9,2 ± 5,3 mmol m^{-2} d^{-1} or 111 ± 64 mg C m^{-2} d^{-1}) reported by Dinauer and Mucci (2017) in spring and summer for the period between 2003-2016 also in the USLE. A compilation of CO_2 flux estimates in 165 estuaries and 87 continental shelves worldwide reveals that, between 23,5 and 50°N, these ecosystems have the largest flux per unit area with a mean F of 23 (± 37) mol m^{-2} y^{-1} or 63 (± 100) mmol m^{-2} d^{-1} (Chen et al. 2013). The KR-USLE continuum (located at 47°N) inserts itself in the lower bracket of these reported values. The CO_2 fluxes reported in this study are likely biased toward low values since the surface pCO_2 measurements were obtained around noon when biological CO_2 uptake (photosynthesis) was presumably maximal. If measurements had been carried out over a full-day cycle (net fluxes), more positive CO_2 emissions would be expected over the whole continuum. These results highlight the spatial and temporal heterogeneity of the KR-USLE continuum, that acts as both a source and a sink of atmospheric CO_2 over different spatial and time scales, yet overall, as a source over the study period. The limited temporal coverage

[1] Multiple units are used here and in the article for comparison purposes.

of surface water pCO_2 in this study prevents these data from being extrapolated reliably to an annual air-sea CO_2 flux, especially in the presence of sea ice in winter when gas exchange is inhibited (Van Der Linden 2020).

1.11 Role of the continuum on the buffering capacity of the receiving coastal waters

In the context of climate change and its effects on marine organisms, it is important to document if continental input exacerbates or mitigates changes to the carbonate system in the coastal ocean (Paulsen et al. 2018, Sippo et al. 2016, Wang et al. 2016). The ratio of TA to DIC (TA/DIC) is of particular interest because it indicates the relative abundance of carbonate species and the system's sensitivity to acidification (Cai et al. 1998, Cai and Wang 1998, Na et al. 2022). At a given temperature and pressure, the buffering capacity of waters to changes in pH, carbonate speciation, as well as calcite and aragonite saturation state ($\mathbf{\Omega}_{Ca}$, $\mathbf{\Omega}_{Ar}$) are closely correlated to this ratio. The buffering capacity of the carbonate system is minimal when the TA and DIC concentrations are equal, and it increases as the ratio gets lower or higher, with the highest acid buffering capacity when TA/DIC > 1 (Egleston et al. 2010).

Surface waters in the Kamouraska River (zone 1) and the USLE (zone 3) had a TA/DIC that is slightly higher than 1 (1,07 ± 0,04 for zone 1 and 1,07 ± 0,02 for zone 3; Table 3) and nearly invariant over the study period. Under these conditions, the surface waters could effectively neutralize released protons from the uptake of atmospheric CO_2, if they were a net sink. The Kamouraska River Estuary (zone 2) waters had a lower buffering capacity, with TA/DIC around 1 in May, July, and August, but the TA/DIC reached a value of 1,17 in October, the highest value recorded in this study. The more acidic summer waters of the Kamouraska River Estuary are partially neutralized upon mixing with the coastal waters of the USLE following the protonation of HCO_3^- to form H_2CO_3 and the loss of CO_2 from the surface waters (Stets et al. 2014), whereas the more alkaline (higher TA/DIC) waters of the continuum in October contribute to the pH buffering capacity of the receiving waters. Whereas the acidity of the surface waters delivered by the Kamouraska River Estuary in the

summer is partially neutralized by the coastal waters of the USLE, the Ω_{Ca} and Ω_{Ar} values show that they remain undersaturated with respect to calcite and aragonite. Upon mixing, the coastal waters of the USLE become supersaturated with respect to calcite ($\Omega_{Ca} > 1$) but remain undersaturated with respect to aragonite ($\Omega_{Ar} < 1$). These saturation state values indicate that, at high-seas slack tide and noon, the ecosystem calcification time window is limited, a process that is essential to certain species (Wahl et al. 2018). As the saturation state data were obtained when the biological CO_2 uptake (photosynthesis) was presumably at its peak, and in surface waters, where the solubility of calcite and aragonite is minimal. Higher saturation state values are to be expected at other times or spatial scales, as observed throughout the year in the Kamouraska River.

1.12 A quantitative but time-specific river-coastal ocean continuum carbon budget

Assuming that the KR-USLE continuum at any given time is in a steady state, the lateral flux of DIC and TA between each zone of the continuum was calculated using the following equation (3):

$$Jx = Cx * D \quad (3)$$

where x is the chemical component (DIC, TA), Jx is the flux of that component (kg C h^{-1} for DIC and µmol h^{-1} for TA), Cx is the mean concentration of the targeted component (kg C l^{-1} for DIC and µmol l^{-1} for TA), and D is the discharge rate of the Kamouraska River (l h^{-1}). Because the measurements were performed at the high-sea slack tide, we roughly estimated that the river discharge propagated along the continuum and mainly drove the downstream transport of surface water and associated solutes from the Kamouraska River to the Kamouraska River Estuary, and from the Kamouraska River Estuary to the USLE. For each sampling day, a mean value of D was extracted from the Kamouraska River hydrometric station (Government of Quebec, 022601). Results of the calculations revealed that the DIC and TA lateral fluxes increased between the Kamouraska River and the Kamouraska River Estuary and from the Kamouraska River Estuary to the USLE (Figure 11). The air-water CO_2

fluxes varied between -0,183 (± 0,013) to 0,136 (± 0,005) kg C h^{-1}, 0,0501 (± 0,1087) to 2,29 (± 0,07) kg C h^{-1}, and -1,33 (± 0,26) to 4,07 (± 2,70) kg C h^{-1} for the Kamouraska River, Kamouraska River Estuary and USLE, respectively (Figure 11). These values represent a snapshot at high-sea slack tide and do not consider the daily variations of the fluxes.

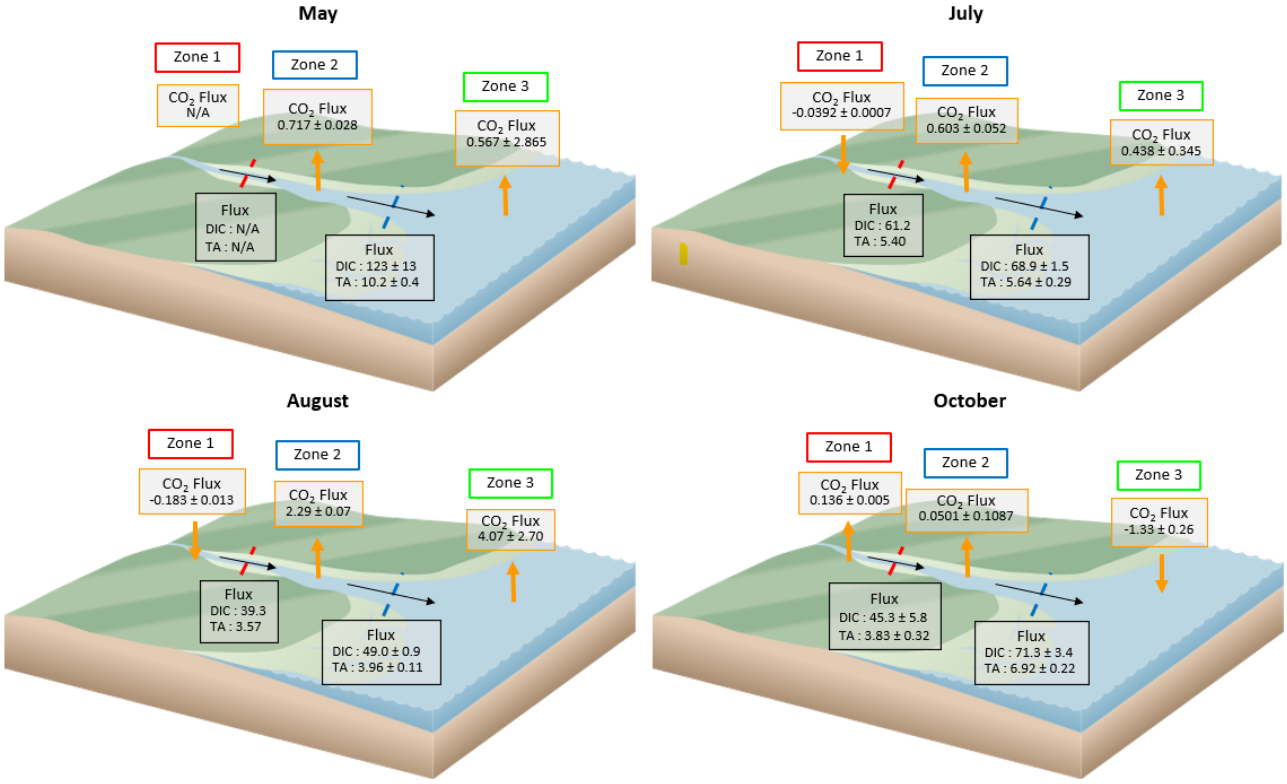

Figure 11. Mean and standard error of the mean of the air-water CO_2 fluxes (kg C h^{-1}) and lateral fluxes of DIC (kg C h^{-1}) and TA (*10^3 mol h^{-1}) along the Kamouraska River to Upper St. Lawrence Estuary continuum during the high-sea slack tide. Values are presented per zone and sampling month. The yellow arrows represent the direction of the air-water fluxes, and the black arrows represent the direction of the lateral fluxes. The red and blue dashed lines are the boundaries between the three zones.

Since the lateral DIC fluxes within the Kamouraska River Estuary and the CO_2 emissions were estimated, it is possible to establish a provisional carbon budget during the high-sea slack tide (see Figure 11). The estimated DIC discharge estimated values (123; 68,9; 49,0 and 71,3 kg C h^{-1} in May, July, August, and October, respectively) are comparable, but lower than rivers with similar size watersheds reported in the literature, such as the Schwabach River (191 m^2 watershed, Germany) and the River Kelvin (331 m^2 watershed, UK), with DIC exports of ~1820 Mg C y^{-1} (Lee et al. 2017) and ~3060 Mg C y^{-1} (Gu et al.

2021), respectively. The lack of data on diel variations limits, however, the upscaling of our results. Nevertheless, they can still provide insights into processes that are active along the continuum. By subtracting the inorganic carbon influx from the outflux in the Kamouraska River Estuary, we obtain that 12%, 23%, and 37% of the inorganic carbon outflux is generated within the Kamouraska River Estuary in July, August, and October, respectively. The non-conservative mixing of DIC concentrations along the KR-USLE continuum (Figure 9) suggests the addition of new inorganic carbon during the transit. Variations of the TA/DIC can also serve as a useful tool to identify the processes producing or consuming inorganic carbon (Borges et al. 2003, Sippo et al. 2016, Urbini et al. 2020).

The ΔTA and ΔDIC of each sample were determined from the differences between their conservative mixing line and the measured concentrations. The ΔTA/ΔDIC were compared to the theoretical ΔTA/ΔDIC produced by selected reactions. The latter are comprised of carbonate dissolution (ΔTA/ΔDIC = 2, R1), carbonate precipitation (ΔTA/ΔDIC = -2, R'1), photosynthesis (ΔTA/ΔDIC = 0,15; R2), aerobic respiration (ΔTA/ΔDIC = -0,15; R'2), nitrate reduction (ΔTA/ΔDIC = 0,8; R3) and sulfate reduction (ΔTA/ΔDIC = 1, R4). Note that the reaction stoichiometries are based on the assumption that the composition of the respired organic matter conforms with the Redfield ratio (C:N:P = 106/16/1), which is not necessarily true in the KR-USLE continuum given the potential various sources of organic matter (terrestrial, marine and freshwater biogenic). The ΔTA/ΔDIC distribution changed over the season (Figure 12). In May, the samples align along a trendline with a slope of 1,10, close to the slope of the anoxic sulfate reduction reaction. During the summer period (in July and August), the slope is close to 0,8, similar to the nitrate reduction reaction. It is interesting to note that ΣNO_3 concentrations in the surface waters were highest during the summer of 2022 along the continuum (5,66 to 44,5 μmol kg^{-1}, Appendix I). In October, however, the slope was 0,17, closer to the slope of the aerobic respiration and photosynthesis reactions, as expected in well-oxygenated waters (160 to 330 μmol l^{-1}, Pers. observation). Hence, variations of ΔTA/ΔDIC imply that the dominant reactions affecting the ratio vary between the seasons. In spring and summer, most of the TA and DIC produced along the continuum apparently originate from suboxic to anoxic

processes (sulfate reduction and nitrate reduction), most likely within the underlying sediment under oxygen-depleted conditions (Cai et al. 2003). The stoichiometric relationship between TA and DIC in the surface water probably results from the degradation of sedimentary organic matter and the subsequent upward diffusion of the catabolic metabolites from the sediment to the overlying water column (Brenner et al. 2016, Diggle et al. 2019, Gustafsson et al. 2019, Thomas et al. 2009).

In October, photosynthesis was the dominant DIC-altering reaction in the surface waters, thus a DIC sink should be expected. However, this sink can be counteracted by the input of DIC from the groundwater. Since the water temperature was lowest in October (Table 3), respiration processes could be limited since their rates are more sensitive to decrease in temperatures than photosynthesis (Marsh et al. 1986, Rasmusson et al. 2020). Thus favoring the latter, especially around noon when the data were collected and photosynthesis was presumably at its maximum (Borges et al. 2003). The production of TA and DIC in spring/summer is concomitant with high F values, indicating a higher DIC production that is released to the atmosphere as well as increasing TA and DIC lateral fluxes to the coastal waters. As the magnitude of F is also dependent on the wind stress, where the weaker wind stress in July limited the exsolution of CO_2, even if pCO_2 gradients at the air-sea interface were higher than in August. In the fall, when the production of DIC is weaker, the amount of CO_2 released to the atmosphere would be lower.

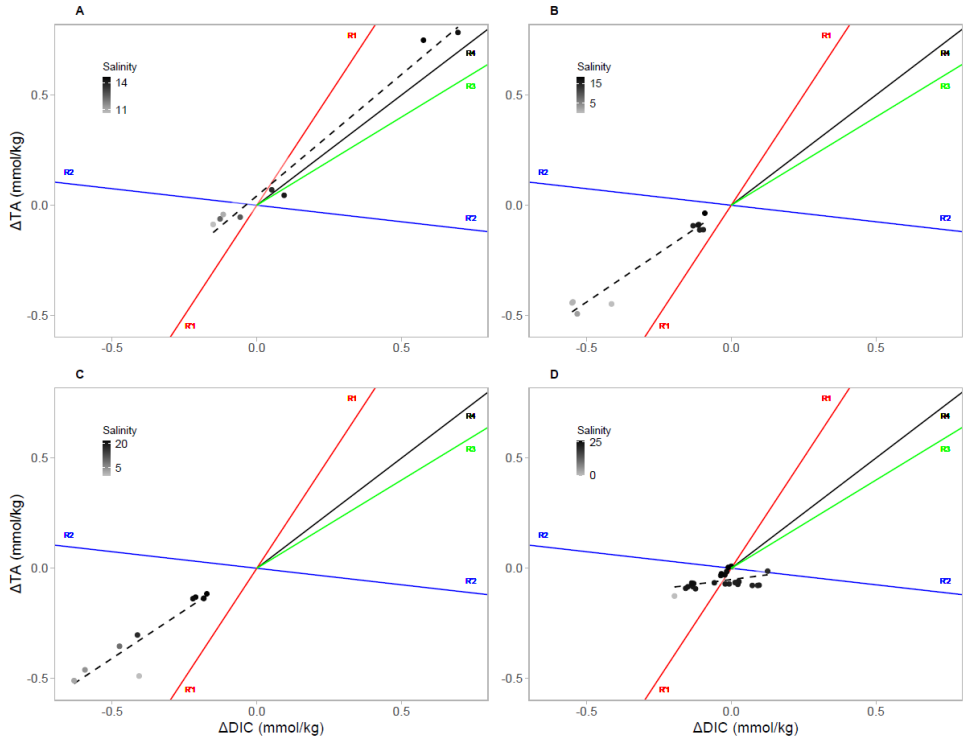

Figure 12. Relationship between ΔTA and ΔDIC (in mmol kg^{-1}). All lines start at the origin (0,0) and indicate the ΔTA/ΔDIC ratio of identified reactions. The red line represents carbonate dissolution (ΔTA/ΔDIC = 2, R1) and carbonate precipitation (ΔTA/ΔDIC = -2, R'1). The blue line represents photosynthesis (ΔTA/ΔDIC = 0,15; R2) and aerobic respiration (ΔTA/ΔDIC = -0,15; R'2). The green line represents nitrate reduction (ΔTA/ΔDIC = 0,8; R3) and the black line represents sulfate reduction (ΔTA/ΔDIC = 1, R4). The greyscale represents the practical salinity value of the sample. The dashed lines are linear least-squares fits to the data. Each sampling month is represented: May (A), July (B), August (C) and October (D).

The δ^{13}C-DIC data provide complementary information on the origin of the DIC and may confirm the role of sedimentary organic matter degradation. The various sources of DIC include: (1) oxidation of organic matter; (2) dissolution of carbonate minerals; (3) exchanges with atmospheric carbon dioxide; and (4) photosynthetic activity (Hélie et al. 2002), all of which can be distinguished from their isotopic composition. In aquatic systems, photosynthetic organisms preferentially use light carbon, which leads to a ^{13}C-DIC enrichment. Photosynthetic activity also contributes to the isotopic composition of the organic carbon stored in the soil and sediment, depending on the dominant photosynthetic cycle. The Kamouraska River watershed is dominated by cereal (wheat, barley, and oats) and fodder production, that comprises C3 plants using the Calvin cycle and produces a strongly depleted ^{13}C organic carbon (mean value of -27‰; Deines, 1980). Carbonate dissolution

typically results in a shift of δ^{13}C-DIC towards slightly positive values (0,20 to 1,10‰; Hillaire-Marcel, 1979), as does CO_2 degassing (Hillaire-Marcel, 1979). The δ^{13}C-DIC values of the surface waters of the continuum are thus a mixture of the DIC produced from organic matter degradation within the continuum and DIC from groundwater, surface runoff, and seawater (high tide). The surface runoff δ^{13}C-DIC signature (-12,20‰) was estimated by extrapolating the data to $S_P = 0$. The seawater δ^{13}C-DIC signature was taken as the value measured from the highest S_P month in the USLE (zone 3, in October, -0,13‰) (Table 3). The groundwater δ^{13}C-DIC composition, if in equilibrium with the limestone in the drainage basin, should have a δ^{13}C-DIC signature of 0 to 1‰ as it was observed by Biehler et al. (2020) in an adjacent Appalachian watershed. The δ^{13}C-DIC signature of the DIC added to the waters along the Kamouraska River Estuary in July, August, and October, was estimated using Keeling plots (Figure 13) and were, respectively, -23,13; -5,06 and 0,24‰. The negative value in July could reflect organic matter degradation and a contribution of CO_2 outgassing pushing that makes the signature a little less negative. The less negative signature in August could be explained by the higher wind stress and thus increased CO_2 outgassing. As for October, the slightly positive δ^{13}C-DIC signature suggests photosynthesis becomes the dominant DIC pool modifying reaction. These findings support the hypothesis proposed previously based on the $\Delta TA/\Delta DIC$ distribution, that the processes that modulate DIC production/consumption along the continuum change over time.

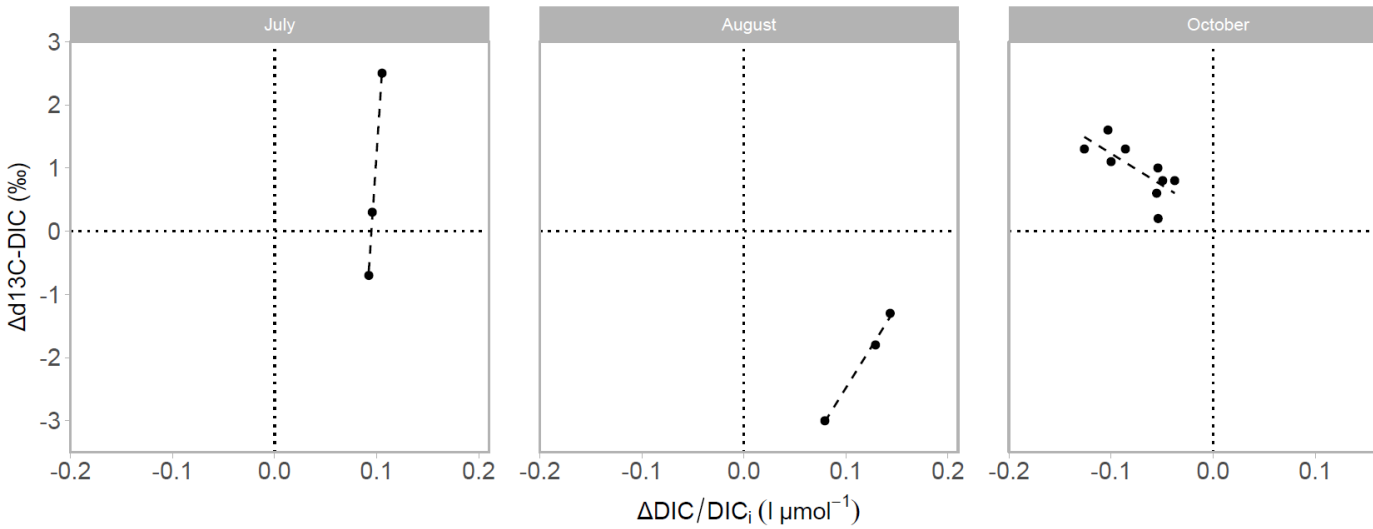

Figure 13. Keeling plot, i.e., $\Delta\delta^{13}$C-DIC (‰) vs ΔDIC/DIC$_i$ (l µmol^{-1}) of the Kamouraska River Estuary from July, August, and October 2022 during the high-sea slack tide. May is not represented because of the lack of freshwater endmember value. $\Delta\delta^{13}$C-DIC and ΔDIC represent the difference between the measured and conservative δ^{13}C-DIC or DIC values. The dashed lines are linear least-squares fits to the data (y = 243x – 23,13, y = 26,1x – 5,06, and y = -9,68 + 0,24 for the months of July, August, and October, respectively). Quadrant I represent primary production/outgassing of CO_2 when DIC concentrations decrease and δ^{13}C-DIC values increase. Quadrant II represents calcite precipitation when DIC concentrations and δ^{13}C-DIC values decrease. Quadrant III represents catabolic degradation of organic carbon when DIC concentrations increase and δ^{13}C-DIC values decrease. Quadrant IV represents carbonate dissolution when the DIC concentrations and the values of δ^{13}C-DIC increase.

CONCLUSIONS

This study investigated the spatial and temporal (seasonal) variability of the carbonate chemistry in the surface waters along the KR-USLE continuum during the high-sea slack tide. While the study provides snapshots of the carbonate chemistry variability throughout the ice-free season and, hence, does not represent the entire variability that could be observed within the continuum. Our results show that the KR-USLE continuum always acted as a source of CO_2 to the atmosphere during the high-sea slack tide, while the river discharge was rapidly mixed with the coastal waters. Although the impact is spatially limited, the DIC and TA inputs still had a negative impact on the buffering capacity on the receiving coastal waters in spring/summer and a positive one in fall. Likewise, the spatial and temporal variability of the DIC and TA inputs contribute to the heterogeneity of the air-sea CO_2 fluxes. The DIC and TA inputs were also quantified in an inorganic carbon budget that identified an important contribution (11,9 to 36,6%) of inorganic carbon from the Kamouraska River Estuary. These

are believed to originate from the diffusion of metabolites generated by catabolic processes in the anoxic sediment in spring/summer and aerobic respiration in the surface waters in the fall. This hypothesis and the seasonal variability are supported by the isotopic composition of the added dissolved inorganic carbon. The temporal variations observed along the surface waters of the KR-USLE continuum are thus mostly driven by the change of dominant biological activities, from organic matter respiration to photosynthesis. This study highlights the need for additional estimates of carbon fluxes in the coastal ocean, under mechanisms underpinning their fluctuations, with an emphasis on land connectivity and surveys at various temporal scales.

CONFLICT OF INTEREST

The authors declare that the research was conducted in the absence of any commercial or financial relationship that could be construed as a potential conflict of interest.

AUTHOR CONTRIBUTIONS

OT planned and carried out the sampling campaigns. OT, FN, AM, and GC participated in discussions of the results presented in this manuscript. OT, FN, AM, and GC wrote and/or provided feedback on the different sections of the manuscript. OT finalized the manuscript for submission. All authors read and approved the submitted version.

ACKNOWLEDGMENTS

The authors thank Carole-Anne Guay, Félix Cloutier-Artiwat, Éléonore Dansereau-Macias, Gwendoline Tommi-Morin, Laísa Peixoto Ramos and Bruno Cayouette for their indispensable help in the field. This project was funded by the *Réseau Québec Maritime* as part of the trans-sectorial project *Odyssée Saint-Laurent « Expertise collective sur l'eutrophisation et la qualité des eaux côtières : vers l'appropriation des connaissances »*.

APPENDIX I

Table 5. Mean and standard error of discrete samples measured nutrients (SRP, ΣNO_3 and DSi) along the continuum. Values are presented per zone and sampling month.

May

Zones	SRP (µmol kg^{-1})	ΣNO_3 (µmol kg^{-1})	DSi (µmol kg^{-1})
1	*N/A*	*N/A*	*N/A*
2	0.20 ± 0.06	14.77 ± 0.42	9.05 ± 0.27
3	0.39 ± 0.05	8.83 ± 2.40	15.82 ± 2.85

July

Zones	SRP (µmol kg^{-1})	ΣNO_3 (µmol kg^{-1})	DSi (µmol kg^{-1})
1	0.32	44.46	43.31
2	0.21 ± 0.14	24.45 ± 7.95	10.51 ± 3.04
3	0.51 ± 0.11	12.48 ± 4.80	19.50 ± 1.00

August

Zones	SRP (µmol kg^{-1})	ΣNO_3 (µmol kg^{-1})	DSi (µmol kg^{-1})
1	0.01	17.61	18.78
2	0.46 ± 0.24	12.55 ± 6.77	6.22 ± 2.59
3	0.67 ± 0.07	5.66 ± 1.94	12.45 ± 3.01

October

Zones	SRP (µmol kg^{-1})	ΣNO_3 (µmol kg^{-1})	DSi (µmol kg^{-1})
1	0.26 ± 0.17	29.78 ± 2.56	63.52 ± 16.73
2	0.87 ± 0.20	9.38 ± 1.53	24.66 ± 3.55
3	0.86 ± 0.10	9.92 ± 1.59	18.78 ± 2.06

CONCLUSION GÉNÉRALE

Ce mémoire a permis d'étudier la dynamique des paramètres du système des carbonates le long du continuum rivière Kamouraska – estuaire supérieur du Saint-Laurent (KR-USLE) à l'étale. Une combinaison de mesures sur le terrain et le calcul des paramètres du système des carbonates a été utilisée afin d'augmenter la précision des calculs dans les eaux douces et côtières. Cette approche combinée, généralement peu utilisée, nécessite une grande quantité d'échantillons et d'analyses mais permet une meilleure compréhension de la dynamique des paramètres du système des carbonates. Plus spécifiquement, elle a permis d'identifier avec plus de précision les processus locaux de production et/ou de consommation du carbone inorganique dans les environnements côtiers. Cette étude a permis d'obtenir des informations essentielles sur le rôle du continuum en tant que puits ou source de CO_2 à l'atmosphère, sur l'impact de la décharge de la rivière Kamouraska sur la capacité tampon du pH des eaux côtières, ainsi que sur son budget de carbone inorganique. Les résultats obtenus montrent les variabilités spatiale et temporelle (saisonnière) des apports et des flux de carbone au sein des environnements côtiers, et souligne le besoin d'inclure des suivis sur diverses échelles spatiales et temporelles pour non seulement établir des bilans régionaux mais aussi pour quantifier la contribution des systèmes côtiers aux bilans globaux de carbone océanique. Afin d'affiner le budget global du carbone, les mesures des paramètres des carbonates devraient s'étaler sur plusieurs heures ou jours, incluant l'ensemble des saisons, tout en couvrant une large superficie, le tout afin de mieux couvrir l'ensemble de la variabilité des environnements côtiers. Une compréhension quantitative de l'océan côtier, à l'échelle locale, est essentiel pour évaluer l'efficacité d'initiatives de remédiation des impacts anthropiques sur les écosystèmes (voir les approches de mCDR, *marine carbone dioxyde removal*). Le budget de carbone inorganique du KR-USLE, pourra servir de base à la compréhension du comportement du système, outil qui pourra être mis à jour et bonifié dans l'avenir.

Les valeurs estimées de flux de CO_2 à l'interface eau-atmosphère tout au long du continuum KR-USLE indiquent qu'il agit globalement d'une source de carbone à

l'atmosphère, tout en présentant des valeurs similaires aux études d'autres petits estuaires au Québec. De plus, la décharge de la rivière Kamouraska a un impact local négatif mineur l'été et positif à l'automne sur la capacité tampon du pH des eaux côtières. Bien que l'influence du continuum KR-USLE sur l'atmosphère et les eaux côtières soit limitée, la forte production de DIC et de TA à l'embouchure de la rivière illustre l'importance de documenter ces processus de production et leur impact au travers du LOAC.

LIMITES DU PROJET

À la suite à cette étude, plusieurs interrogations demeurent. Bien que les résultats permettent d'illustrer et partiellement élucider la dynamique des paramètres du système des carbonates du continuum rivière Kamouraska – estuaire supérieur du Saint-Laurent à l'étale, certains aspects de ces variations n'ont pas pu être explorés. En effet, il serait, par exemple, pertinent d'étudier l'impact de l'onde de marée sur la dynamique des paramètres du système des carbonates le long du continuum, d'inclure des valeurs hivernales, ainsi que des valeurs nocturnes afin de couvrir une plus large plage des variations temporelles. Afin de bonifier le budget carbone du continuum KR-USLE, il serait nécessaire de quantifier la décharge d'eau souterraine par le développement d'un bilan de masse du radon (^{222}Rn, $T_{1/2}$ = 3,82 jours) via des mesures *in situ* en continu de ^{222}Rn. Le ^{222}Rn est un isotope radioactif naturel issu de la dégradation de son isotope parent, le radium (^{226}Ra) dans les eaux souterraines. Son comportement conservatif et chimiquement stable, combiné avec son activité accrue dans les eaux souterraines, en comparaison aux eaux de surface, permet son utilisation comme traceur des échanges entre les eaux souterraines et les eaux de surface (Burnett et al. 2010). Les apports d'eau souterraine et de carbone inorganique dissout peuvent être considérables et la quantification de ces apports permettrait de préciser la contribution de la production interne de DIC et TA à l'estuaire de la rivière Kamouraska.

Afin de mieux identifier l'origine du DIC et TA observés à l'embouchure de la rivière Kamouraska, il serait aussi pertinent d'analyser les eaux porales des sédiments de l'embouchure, afin de déterminer les concentrations ainsi que les flux à l'interface eau-

sédiment de DIC, TA, ammonium (NH_4^+) et sulfure d'hydrogène (HS^-). La présence de ces derniers composés est un indicateur de la réduction de nitrates (pour le NH_4^+) et de la réduction de sulfates (pour le HS^-) ce qui permettrait de confirmer la présence de ces processus dans la production interne de DIC et TA dans l'estuaire de la rivière Kamouraska. En effet, le compartiment sédimentaire a complètement été omis des calculs des flux entre les zones du continuum à cause de l'absence de données. Cependant, nos résultats montrent également que sans une bonne caractérisation de ce compartiment, les processus ne peuvent pas tous être expliqués.

PERSPECTIVES

Afin de pousser l'étude du continuum KR-USLE plus loin, il serait pertinent d'évaluer la variation journalière à fine échelle des flux de CO_2 à l'interface air-eau, afin d'obtenir un flux net de CO_2 journalier. Ceci permettrait d'améliorer la compréhension du comportement du système à l'échelle d'un cycle journalier, spécifiquement l'influence des apports des eaux continentales aux eaux côtières, mais également des processus biogéochimiques tout au long du LOAC. La décision, qui a été prise pour cette étude, d'effectuer les mesures sur le terrain à l'étale, a permis d'évaluer la variation saisonnière du continuum KR-USLE, mais a mis de côté la variation journalière. Ces informations seraient donc complémentaires à l'étude actuelle, permettant d'avoir une vision plus complète (journalière et saisonnière) des variations des paramètres du système des carbonates et, plus spécifiquement, des flux de ces paramètres. Puisque cette étude s'inscrit dans l'approfondissement des connaissances de la dynamique des paramètres du système des carbonates en écosystèmes côtiers, l'ajout de l'observation des variations journalières pourrait contribuer à la mise en lumière de l'importante hétérogénéité de ces milieux. Cet apport contribuerait également à l'affinement du bilan carbone à l'échelle locale, nécessaire afin d'avoir un bilan carbone global représentatif de l'hétérogénéité de ces échelles locales.

RÉFÉRENCES BIBLIOGRAPHIQUES

Abril G, Borges AV. 2005. Carbon dioxide and methane emissions from estuaries. Pages 187-207. Greenhouse gas emissions—fluxes and processes: hydroelectric reservoirs and natural environments, *Springer*.

Abril G, et al. 2015. Technical Note: Large overestimation of pCO_2 calculated from pH and alkalinity in acidic, organic-rich freshwaters. *Biogeosciences* 12: 67-78.

Abril G, Etcheber H, Borges AV, Frankignoulle M. 2000. Excess atmospheric carbon dioxide transported by rivers into the Scheldt estuary. Comptes rendus de l'Académie des sciences. Série 2, Sciences de la terre et des planètes 330 (11): 761-768.

Bauer JE, Cai W-J, Raymond PA, Bianchi TS, Hopkinson CS, Regnier PAG. 2013. The changing carbon cycle of the coastal ocean. *Nature* 504: 61-70.

Biehler A, Buffin-Bélanger T, Baudron P, Chaillou G. 2023. Groundwater discharge contribution to dissolved inorganic carbon and riverine carbon emissions in a subarctic region. *Biogeochemistry* 165: 129-150.

Biehler A, Chaillou G, Buffin-Bélanger T, Baudron P. 2020. Hydrological connectivity in the aquifer–river continuum: Impact of river stages on the geochemistry of groundwater floodplains. *Journal of Hydrology*, 590, 125379.

Borges AV. 2005. Do we have enough pieces of the jigsaw to integrate CO_2 fluxes in the coastal ocean? *Estuaries* 28: 3-27.

Borges AV, Delille B, Frankignoulle M. 2005. Budgeting sinks and sources of CO_2 in the coastal ocean: Diversity of ecosystems counts. *Geophysical Research Letters* 32: L14601.

Borges AV, Djenidi S, Lacroix G, Théate J, Delille B, Frankignoulle M. 2003. Atmospheric CO2 flux from mangrove surrounding waters. *Geophysical Research Letters* 30 (11): 1558.

Bourgeois T, Orr JC, Resplandy L, Terhaar J, Ethé C, Gehlen M, Bopp L. 2016. Coastal-ocean uptake of anthropogenic carbon. *Biogeosciences* 13: 4167-4185.

Boyd PW, et al. 2018. Experimental strategies to assess the biological ramifications of multiple drivers of global ocean change—A review. *Global Change Biology* 24: 2239-2261.

Brenner H, Braeckman U, Le Guitton M, Meysman FJR. 2016. The impact of sedimentary alkalinity release on the water column CO_2 system in the North Sea. *Biogeosciences* 13: 841-863.

Burnett WC, Peterson RN, Santos IR, Hicks RW. 2010. Use of automated radon measurements for rapid assessment of groundwater flow into Florida streams. *Journal of Hydrology* 380: 298-304.

Cai W-J. 2011. Estuarine and Coastal Ocean Carbon Paradox: CO_2 Sinks or Sites of Terrestrial Carbon Incineration? *Annual Review of Marine Science* 3: 123-145.

Cai W-J, Dai M. 2004. Comment on "Enhanced Open Ocean Storage of CO_2 from Shelf Sea Pumping". *Science* 306: 1477.

Cai W-J, Dai M, Wang Y. 2006. Air-sea exchange of carbon dioxide in ocean margins: A province-based synthesis. *Geophysical Research Letters* 33: L12603.

Cai W-J, et al. 2011. Acidification of subsurface coastal waters enhanced by eutrophication. *Nature Geoscience* 4: 766-770.

Cai W-J, Wang Y. 1998. The chemistry, fluxes, and sources of carbon dioxide in the estuarine waters of the Satilla and Altamaha Rivers, Georgia. *Limnology and Oceanography* 43: 657-668.

Cai W-J, Wang Y, Hodson RE. 1998. Acid-Base Properties of Dissolved Organic Matter in the Estuarine Waters of Georgia, USA. *Geochimica et Cosmochimica Acta* 62 (3): 473-483.

Cai W-J, Wang Y, Krest J, Moore WS. 2003. The geochemistry of dissolved inorganic carbon in a surficial groundwater aquifer in North Inlet, South Carolina, and the carbon fluxes to the coastal ocean. *Geochimica et Cosmochimica Acta* 67 (4): 631-637.

Cai W-J, et al. 2020. Controls on surface water carbonate chemistry along North American ocean margins. *Nature Communications* 11 (1): 2691.

Campeau A, Lapierre JF, Vachon D, Del Giorgio PA. 2014. Regional contribution of CO_2 and CH_4 fluxes from the fluvial network in a lowland boreal landscape of Québec. *Global Biogeochemical Cycles* 28: 57-69.

Chen C-TA, Borges AV. 2009. Reconciling opposing views on carbon cycling in the coastal ocean: Continental shelves as sinks and near-shore ecosystems as sources of atmospheric CO_2. *Deep Sea Research Part II: Topical Studies in Oceanography* 56: 578-590.

Chen C-TA, Huang T-H, Chen Y-C, Bai Y, He X, Kang Y. 2013. Air–sea exchanges of CO_2 in the world's coastal seas. *Biogeosciences* 10: 6509-6544.

Chen C-TA, Wang S-L. 1999. Carbon, alkalinity and nutrient budgets on the East China Sea continental shelf. *Journal of Geophysical Research: Oceans* 104: 20675-20686.

Cole JJ, et al. 2007. Plumbing the Global Carbon Cycle: Integrating Inland Waters into the Terrestrial Carbon Budget. *Ecosystems* 10: 172-185.

Dai M, Cao Z, Guo X, Zhai W, Liu Z, Yin Z, Xu Y, Gan J, Hu J, Du C. 2013. Why are some marginal seas sources of atmospheric CO_2? *Geophysical Research Letters* 40: 2154-2158.

Dai M, et al. 2022. Carbon Fluxes in the Coastal Ocean: Synthesis, Boundary Processes, and Future Trends. *Annual Review of Earth and Planetary Sciences* 50: 593-626.

Deines P. 1980. The isotopic composition of reduced organic carbon. Handbook of Environmental Isotope Geochemistry.

Delaigue L, Thomas H, Mucci A. 2020. Spatial variations in CO_2 fluxes in the Saguenay Fjord (Quebec, Canada) and results of a water mixing model. *Biogeosciences* 17: 547-566.

Dickson A. 1981. An exact definition of total alkalinity and a procedure for the estimation of alkalinity and total inorganic carbon from titration data. *Deep Sea Research Part A. Oceanographic Research Papers* 28 (6): 609-623.

Dickson A. 1990. Standard potential of the reaction: AgCl(s) +1/2H_2(g) + HCl(aq), and the standard acidity constant of the ion HSO_4^- in synthetic sea water from 273.15 to 318.15 K. *The Journal of Chemical Thermodynamics* 22: 113-127.

Diggle RM, Tait DR, Maher DT, Huggins X, Santos IR. 2019. The role of porewater exchange as a driver of CO_2 flux to the atmosphere in a temperate estuary (Squamish, Canada). *Environmental Earth Sciences* 78: 336.

Dinauer A, Mucci A. 2017. Spatial variability in surface-water pCO_2 and gas exchange in the world's largest semi-enclosed estuarine system: St. Lawrence Estuary (Canada). *Biogeosciences* 14: 3221-3237.

Douglas N, Byrne R. 2017. Spectrophotometric pH measurements from river to sea: Calibration of mCP for 0 S 40 and 278.15 T 308.15 K. *Marine Chemistry* 197: 64-69.

Egleston ES, Sabine CL, Morel FMM. 2010. Revelle revisited: Buffer factors that quantify the response of ocean chemistry to changes in DIC and alkalinity. *Global Biogeochemical Cycles* 24: GB1002.

Feely RA, Sabine CL, Lee K, Berelson W, Kleypas JA, Fabry VJ, Millero FJ. 2004. Impact of anthropogenic CO_2 on the $CaCO_3$ system in the oceans. *Science* 305: 362-366.

Gruber N, et al. 2019. The oceanic sink for anthropogenic CO_2 from 1994 to 2007. *Science* 363: 1193-1199.

Gruber N, Gloor M, Mikaloff Fletcher SE, Doney SC, Dutkiewicz S, Follows MJ, Gerber M, Jacobson AR, Joos F, Lindsay K. 2009. Oceanic sources, sinks, and transport of atmospheric CO_2. *Global Biogeochemical Cycles* 23: GB1005.

Gu C, Waldron S, Bass AM. 2021. Carbon dioxide, methane, and dissolved carbon dynamics in an urbanized river system. *Hydrological Processes* 35: e14360.

Guo X-H, Zhai W-D, Dai M-H, Zhang C, Bai Y, Xu Y, Li Q, Wang G-Z. 2015. Air–sea CO_2 fluxes in the East China Sea based on multiple-year underway observations. *Biogeosciences* 12: 5495-5514.

Gustafsson E, Hagens M, Sun X, Reed DC, Humborg C, Slomp CP, Gustafsson BG. 2019. Sedimentary alkalinity generation and long-term alkalinity development in the Baltic Sea. *Biogeosciences* 16: 437-456.

Hélie JF, Hillaire-Marcel C, Rondeau B. 2002. Seasonal changes in the sources and fluxes of dissolved inorganic carbon through the St. Lawrence Riverisotopic and chemical constraint. *Chemical Geology* 186: 117-138.

Hillaire-Marcel C. 1979. Les mers post-glaciaires du Québec: Quelques aspects. Doctoral Thesis, Université Pierre et Marie Curie, Paris VI, 2 volumes.

Hofmann GE, Smith JE, Johnson KS, Send U, Levin LA, Micheli F, Paytan A, Price NN, Peterson B, Takeshita Y. 2011. High-frequency dynamics of ocean pH: a multi-ecosystem comparison. *PLOS ONE* 6: e28983.

Hunt CW, Salisbury JE, Vandemark D, McGillis W. 2011. Contrasting Carbon Dioxide Inputs and Exchange in Three Adjacent New England Estuaries. *Estuaries and Coasts* 34: 68-77.

IPCC. 2014. Climate Change 2014: Synthesis Report. Contribution of Working Groups I, II and III to the Fifth Assessment Report of the Intergovernmental Panel on Climate Change [Core Writing Team, R.K. Pachauri and L.A. Meyer (eds.)]. IPCC, Geneva, Switzerland, 151 pp.

IPCC. 2022: Climate Change 2022: Impacts, Adaptation and Vulnerability. Contribution of Working Group II to the Sixth Assessment Report of the Intergovernmental Panel on Climate Change [H.-O. Pörtner, D.C. Roberts, M. Tignor, E.S. Poloczanska, K. Mintenbeck, A. Alegría, M. Craig, S. Langsdorf, S. Löschke, V. Möller, A. Okem, B. Rama (eds.)]. *Cambridge University Press.* Cambridge University Press, Cambridge, UK and New York, NY, USA, 3056 pp.

Julliard C, Noisette F, Winkler G, Nozais C. 2023. Trajectoire d'eutrophisation de la zone côtière du Kamouraska : approches biologiques et physico-chimiques. Master's Thesis, Université du Québec à Rimouski, 80 pp.

Keeling RF, Manning AC. 2014. Studies of recent changes in atmospheric O_2 content. Pages 385-404. *Treatise on Geochemistry 2nd Edition* Vol. 5: 385-404.

Kuliński K, Schneider B, Hammer K, Machulik U, Schulz-Bull D. 2014. The influence of dissolved organic matter on the acid–base system of the Baltic Sea. *Journal of Marine Systems* 132: 106-115.

Lacroix F, Ilyina T, Laruelle GG, Regnier P. 2021. Reconstructing the preindustrial coastal carbon cycle through a global ocean circulation model: was the global continental shelf already both autotrophic and a CO_2 sink? *Global Biogeochemical Cycles* 35: e2020GB006603.

Laruelle GG, Lauerwald R, Pfeil B, Regnier P. 2014. Regionalized global budget of the CO_2 exchange at the air-water interface in continental shelf seas. *Global Biogeochemical Cycles* 28: 1199-1214.

Laruelle GG, Lauerwald R, Rotschi J, Raymond PA, Hartmann J, Regnier P. 2015. Seasonal response of air–water CO_2 exchange along the land–ocean aquatic continuum of the northeast North American coast. *Biogeosciences* 12: 1447-1458.

Lee K, Van Geldern R, Barth JAC. 2017. A high-resolution carbon balance in a small temperate catchment: Insights from the Schwabach River, Germany. *Applied Geochemistry* 85: 86-96.

Lee K, Kim T-W, Byrne RH, Millero FJ, Feely RA, Liu Y-M. 2010. The universal ratio of boron to chlorinity for the North Pacific and North Atlantic oceans. *Geochimica et Cosmochimica Acta* 74: 1801-1811.

Li Q, Guo X, Zhai W, Xu Y, Dai M. 2020. Partial pressure of CO_2 and air-sea CO_2 fluxes in the South China Sea: Synthesis of an 18-year dataset. *Progress in Oceanography* 182: 102272.

Marsh JA, Dennison WC, Alberte RS. 1986. Effects of temperature on photosynthesis and respiration in eelgrass (*Zostera marina L.*). *Journal of Experimental Marine Biology and Ecology* 101: 257-267.

Meybeck M. 1982. Carbon, nitrogen, and phosphorus transport by world rivers. *American Journal of Science* 282: 401-450.

Middelburg JJ, Soetaert K, Hagens M. 2020. Ocean Alkalinity, Buffering and Biogeochemical Processes. *Reviews of Geophysics* 58: e2019RG000681.

Na T, Hwang J, So-Yun K, Jeong S, Rho T, Lee T. 2022. Large Increase in Dissolved Inorganic Carbon in the East Sea (Japan Sea) From 1999 to 2019. *Frontiers in Marine Science* 9: 825206.

Paulsen M-L, et al. 2018. Temporal Changes in Seawater Carbonate Chemistry and Carbon Export from a Southern California Estuary. *Estuaries and Coasts* 41: 1050-1068.

Perez FF, Fraga F. 1987. Association constant of fluoride and hydrogen ions in seawater. *Marine Chemistry* 21: 161-168.

Pierrot D, Epitalon J-M, Orr JC, Lewis E, and Wallace DWR. MS Excel program developed for CO_2 system calculations – version 3.0, (2021), GitHub repository, https://github.com/dpierrot/co2sys_xl.

Poisson A, et al. 1993. Variability of sources and sinks of CO_2 in the western Indian and southern oceans during the year 1991. *Journal of Geophysical Research: Oceans* 98: 22759-22778.

R Core Team. 2022. R: A language and environment for statistical computing. R Foundation for Statistical Computing, Vienna, Austria. URL https://www.R-project.org/.

Rasmusson LM, Buapet P, George R, Gullström M, Gunnarsson PCB, Björk M. 2020. Effects of temperature and hypoxia on respiration, photorespiration, and photosynthesis of seagrass leaves from contrasting temperature regimes. *ICES Journal of Marine Science* 77: 2056-2065.

Regnier P, et al. 2013. Anthropogenic perturbation of the carbon fluxes from land to ocean. *Nature Geoscience* 6: 597-607.

Regnier P, Resplandy L, Najjar RG, Ciais P. 2022. The land-to-ocean loops of the global carbon cycle. *Nature* 603: 401-410.

Robert-Baldo GL, Morris MJ, Byrne RH. 1985. Spectrophotometric determination of seawater pH using phenol red. *Analytical Chemistry* 57: 2564-2567.

Roobaert A, Laruelle GG, Landschützer P, Gruber N, Chou L, Regnier P. 2019. The Spatiotemporal Dynamics of the Sources and Sinks of CO_2 in the Global Coastal Ocean. *Global Biogeochemical Cycles* 33: 1693-1714.

Roobaert A, Resplandy L, Laruelle GG, Liao E, Regnier P. 2022. A framework to evaluate and elucidate the driving mechanisms of coastal sea surface CO_2 seasonality using an ocean general circulation model (MOM6-COBALT). *Ocean Science* 18: 67-88.

Sabine CL, et al. 2004. The Oceanic Sink for Anthropogenic CO_2. *Science* 305: 367-371.

Sippo JZ, Maher DT, Tait DR, Holloway C, Santos IR. 2016. Are mangroves drivers or buffers of coastal acidification? Insights from alkalinity and dissolved inorganic carbon export estimates across a latitudinal transect. *Global Biogeochemical Cycles* 30: 753-766.

Soetaert K, Hofmann AF, Middelburg JJ, Meysman FJ, Greenwood J. 2007. Reprint of "The effect of biogeochemical processes on pH". *Marine Chemistry* 106: 380-401.

Song S, Wang ZA, Gonneea ME, Kroeger KD, Chu SN, Li D, Liang H. 2020. An important biogeochemical link between organic and inorganic carbon cycling: Effects of organic alkalinity on carbonate chemistry in coastal waters influenced by intertidal salt marshes. *Geochimica et Cosmochimica Acta* 275: 123-139.

Sournia A. 1975. Circadian Periodicities in Natural Populations of Marine Phytoplankton. *Advances in Marine Biology* 12: 325-389.

St-Laurent P, Friedrichs MAM, Najjar RG, Shadwick EH, Tian H, Yao Y. 2020. Relative impacts of global changes and regional watershed changes on the inorganic carbon balance of the Chesapeake Bay. *Biogeosciences* 17: 3779-3796.

Stets E, Kelly V, Crawford C. 2014. Long-term trends in alkalinity in large rivers of the conterminous US in relation to acidification, agriculture, and hydrologic modification. *Science of The Total Environment* 488-489: 280-289.

Teodoru CR, Del Giorgio PA, Prairie YT, Camire M. 2009. Patterns in pCO_2 in boreal streams and rivers of northern Quebec, Canada. *Global Biogeochemical Cycles* 23: GB2012.

Thomas H, Bozec Y, Elkalay K, De Baar HJW. 2004. Enhanced Open Ocean Storage of CO_2 from Shelf Sea Pumping. *Science* 304: 1005-1008.

Thomas H, Schiettecatte LS, Suykens K, Koné YJM, Shadwick EH, Prowe AEF, Bozec Y, De Baar HJW, Borges AV. 2009. Enhanced ocean carbon storage from anaerobic alkalinity generation in coastal sediments. *Biogeosciences* 6: 267-274.

Tommi-Morin G, Chaillou G, Bélanger S. 2022. Les estuaires souterrains en milieu transgressif : source d'acidification à l'océan côtier, Master's Thesis, Université du Québec à Rimouski, 70 pp.

Urbini L, Ingrosso G, Djakovac T, Piacentino S, Giani M. 2020. Temporal and Spatial Variability of the CO_2 System in a Riverine Influenced Area of the Mediterranean Sea, the Northern Adriatic. *Frontiers in Marine Science* 7: 679.

Van Der Linden FC, Tison J -L, Champenois W, Moreau S, Carnat G, et al.. 2020. Sea Ice CO_2 Dynamics Across Seasons: Impact of Processes at the Interfaces. *Journal of Geophysical Research: Oceans*. 125: e2019JC01580.

Wahl M, Schneider Covachã S, Saderne V, Hiebenthal C, Müller JD, Pansch C, Sawall Y. 2018. Macroalgae may mitigate ocean acidification effects on mussel calcification by increasing pH and its fluctuations. *Limnology and Oceanography* 63: 3-21.

Wang ZA, Kroeger KD, Ganju NK, Gonneea ME, Chu SN. 2016. Intertidal salt marshes as an important source of inorganic carbon to the coastal ocean. *Limnology and Oceanography* 61: 1916-1931.

Wanninkhof R. 2014. Relationship between wind speed and gas exchange over the ocean revisited. *Limnology and Oceanography: Methods* 12: 351-362.

Willeit M, Ganopolski A, Calov R, Brovkin V. 2019. Mid-Pleistocene transition in glacial cycles explained by declining CO2 and regolith removal. *Science Advances* 5: eaav7337.

Wolf-Gladrow DA, Zeebe RE, Klaas C, Körtzinger A, Dickson AG. 2007. Total alkalinity: The explicit conservative expression and its application to biogeochemical processes. *Marine Chemistry* 106: 287-300.

Zeebe RE. 2012. History of Seawater Carbonate Chemistry, Atmospheric CO_2, and Ocean Acidification. *Annual Review of Earth and Planetary Sciences* 40: 141-165.

Zeebe RE, Ridgwell A. 2011. Past changes of ocean carbonate chemistry. *Ocean acidification, Chapter* 2: 1-28.

Zeebe RE, Wolf-Gladrow D. 2001. CO_2 in seawater: equilibrium, kinetics, isotopes. Gulf Professional Publishing.